

Article

Geology and Mineralogy of Rare Earth Elements Deposits and Occurrences in Finland

Thair Al-Ani ^{1,*}, Ferenc Molnár ¹ , Panu Lintinen ² and Seppo Leinonen ³¹ Geological Survey of Finland (GTK), Betonimiehenkuja 4, FI-02151 Espoo, Finland; ferenc.molnar@gtk.fi² Geological Survey of Finland (GTK), Lähteentie 2, FI-96101 Rovaniemi, Finland; panu.lintinen@gtk.fi³ Geological Survey of Finland (GTK), Neulaniementie 5, FI-70211 Kuopio, Finland; seppo.leinonen@gtk.fi

* Correspondence: thair.alani@gtk.fi; Tel.: +358-40-550-9479

Received: 3 June 2018; Accepted: 5 July 2018; Published: 18 August 2018



Abstract: Rare earth elements (REE) have critical importance in the manufacturing of many electronic products in the high-tech and green-tech industries. Currently, mining and processing of REE is strongly concentrated in China. A substantial growth in global exploration for REE deposits has taken place in the recent years and has resulted in considerable advances in defining new resources. This study provides an overview of the mineralogical and petrological peculiarities of the most important REE prospects and metallogeny of REE in Finland. There is a particularly good potential for future discoveries of carbonatite hosted REE deposits in the Paleozoic Sokli carbonatite complex, as well as in the Paleoproterozoic Korsnäs and Kortejärvi Laivajoki areas. This review also provides information about the highest known REE concentration in the alkaline intrusions of Finland in the Tana Belt and other alkaline rock hosted occurrences (e.g., Otanmäki and Katajakangas). Significant REE enrichments in hydrothermal alteration zones are also known in the Kuusamo Belt (Uuniniemi and Honkilehto), and occurrences of REE-rich mineralisation are also present in granite pegmatite bodies and greisens in central and southern Finland (Kovela monazite granite and the Rapakivi Granite batholith at Vyborg, respectively). REE minerals in all of the localities listed above were identified and analyzed by scanning electron microscopy (SEM) and electron microprobes (EMPs). In localities of northern and central Finland, both primary rock forming and epigenetic-hydrothermal REE minerals were found, namely phosphates (monazite-Ce, xenotime-Y), fluorcarbonates (bastnäsite-Ce, synchysite), and hydrated carbonates (ancylite-Ce), hydrated aluminium silicates (allanite-Ce, Fe-allanite, cerite, chevkinite), oxides (fergusonite, euxenite) and U-Pb rich minerals. The chondrite normalized REE concentrations, the La/Nd ratios and the REE vs. major element contents in several types of REE bearing minerals from prospects in Finland can be used to identify and define variable REE fractionation processes (carbonatites), as well as to discriminate deposits of different origins.

Keywords: REE enrichments in carbonatite and alkaline rocks; REE in hydrothermal alteration zones and granitic rocks; REE mineralogy; crystal-chemistry of REE minerals; Finland

1. Introduction

The demand for rare earth elements has spiked in recent years due to their increasing usage in numerous high-technology applications that touch many aspects of modern life and culture. Specific REEs are used individually or in combination to make phosphors—substances that emit luminescence—for many types of ray tubes and flat panel displays, in screens that range in size from smart phone displays to stadium scoreboards. Some REEs are used in fluorescent and LED lighting. Yttrium, europium, and terbium phosphors are the red-green-blue phosphors used in many light bulbs, panels, and televisions.

Enrichment of the REE may occur through primary processes such as magmatic processes and hydrothermal fluid mobilization and precipitation, or through secondary processes that move REE minerals from where they originally formed, such as sedimentary concentration and weathering. Natural rare earth element deposits and occurrences may thus be divided into primary (high-temperature) and secondary (low-temperature) deposit types. The most important primary deposits with high grade and tonnage are typically associated with alkaline-peralkaline igneous rocks and carbonatites formed in extensional intracontinental rifts [1,2].

Today, almost all (~98%) of the world's REE supply comes from China, with 40%–50% of this production contributed by the giant Fe-REE-Nb deposit at Bayan Obo [3,4]. These rich ores are dominated by light rare earth elements (e.g., [2–6]). Reserves are estimated at more than 40 million tons of REE minerals grading at 3–5.4 wt % REE (70% of world's known REE reserves), 1 million tons of Nb₂O₅ and 470 million tons of iron. The deposit also contains an estimated 130 million tons of fluorite [2,6]. REE deposits associated with alkaline igneous rocks are typically lower grade but with larger tonnage and a higher content of HREE [2]. The other sources are minor and, in addition to the Mountain Pass bastnäsite and Russian loparite eudialyte deposits, include placers, where monazite and xenotime are extracted as by-products from ilmenite-zircon sands (India, Brazil, Malaysia). Since 2003, none of these sources have contributed more than 3.5 thousand metric tons (kt) rare earth oxides (REO) (i.e., <3% of global output).

The main REE metallogenic provinces in Europe are those areas where extensional tectonics and introduction of enriched mantle melts into shallow crustal levels have produced alkaline silicate and carbonatite intrusions. The major REE deposits are currently known in those areas where those intrusions have been exposed by erosion [7]. The most notable REE deposits are found in the Mesoproterozoic Gardar Province of south-west Greenland [8], and the Protogine Zone, a major, multiply reactivated, in part extensional structure in southern Sweden [9]. The majority of the Kola Alkaline Province lies in Russia, where it contains significant REE deposits in the Lovozero and Khibiny intrusive complexes [10]. Mineral deposits of REE in the nepheline syenites and foidolites of the Lovozero plutons have 7.1 million tons (Mt) resources with 1.12 wt % average REO content, whereas in the apatite-nepheline rocks of Khibiny complex, 5.5 Mt REO resources with 0.40 wt %, average REO content are known [10,11]. The westernmost part of the province falls within the Finnish border, with two main intrusions: the Sokli phoscorite-carbonatite complex, and the Iivaara alkaline complex (Figure 1). The approximately 360–380 Ma old Sokli carbonatite complex in north eastern Finland hosts a deeply weathered and unexploited phosphate deposit, which is enriched in niobium (Nb), tantalum (Ta), zirconium (Zr), REE and uranium (U). The Sokli complex shows many important similarities to other alkaline complexes of the Devonian Kola alkaline province, especially to the Kovdor and to the Vuorijärvi complexes (in Russia). These similarities include occurrences of early stage ultramafic cumulate rocks, well-developed phoscorite-carbonatite associations and late stage carbonatites that represent evolution of carbonate magmas from dolomite carbonatites to final stage light rare earth element (LREE)-Sr-Ba dolomite carbonatite pulses. However, a critically important difference at Sokli is the vastly greater abundance of carbonatite relative to the cumulate ultramafic rocks. Exploration for REE by the Geological Survey of Finland in the Sokli complex has focused on the fenite aureole and associated late-stage, crosscutting carbonatite dikes that seem to have the highest potential for REE mineralization [12]. The ore reserve in the “soft-rock” phosphate-rich materials is about 114 Mt with 15 wt % P₂O₅ content with an additional, approximately 75 Mt resources in the weathered bedrock containing about 5.6 wt % P₂O₅. Iivaara is the type locality of ijolite, which is a common rock type in carbonatite-bearing alkaline complexes. The phosphor potential of the Iivaara intrusion is very high, but the REE potential is still under study. The Iivaara intrusion shows many similarities with the Lovozero alkaline massif in Russia. Results of the previous mineralogical studies in samples from historic drill cores indicate that the Iivaara nepheline-syenite contains apatite and a small amount of allanite. The samples contain 1%–5% P₂O₅ and 200 ppm REE only [13]. Other examples of alkaline magmatic rock occurrences include the c. 2600 Ma Siilinjärvi carbonatite complex [14,15];

and the c. 2050 Ma Katajakangas alkaline gneiss [12,16]. Apatite is currently mined at Siilinjärvi as a phosphate resource. The main rock types at Siilinjärvi are enriched in REE, and REE-hosting minerals in the carbonatite and associated “glimmerite” include monazite-(Ce), pyrochlore-group minerals, LREE-bearing strontianite and REE-bearing Ti, Nb-phases [17]. The Katajakangas gneiss contains mineralised layers, which are rich in zircon, bastnäsite, columbite, and thorite, and an informal resource estimate indicate 0.46 Mt ore with 2.4% average total rare earth oxides [16].

This paper presents an overview of the main REE occurrences and prospects in Finland, and identifies areas with the most significant potential for future exploration and development, on the basis of their geological suitability. In addition to a detailed geological description of the potential areas, mineralogy of occurrences and prospects are also fully characterized as beneficiation methods have to be tailor-made for each deposit, and are dependent on properties such as mineralogy, textures, and grain size of the ore. Results of geochemical and mineralogical studies on samples from new drillings completed by the Geological Survey of Finland between 2009 and 2016 are also included in this review. Mineralogical studies of samples from the new drill cores were focused on the following exploration targets: (1) the fenitic zone surrounding the Sokli carbonatite intrusions at Jammi and Kaulus; (2) the Pb-REE occurrence hosted by calcsilicate rocks and dikes of carbonatite at Korsnäs; (3) the Kortejärvi carbonatite and Laivajoki silicocarbonatite complexes; (4) the alkaline gneissic granite in the Otanmäki area; (5) the REE-Au mineralization at Mäkärä and Vaulo in the Tana Belt; (6) the metasomatic-hydrothermal Au-Co-Cu-Fe-U and REE deposits with intense albitization in the Kuusamo belt; (7) the Kovala monazite granite in southern Finland and (8) the Vybörg rapakivi granite batholith in south eastern Finland. Here we classify these deposits and occurrences on the basis of their origin and geological settings (Figure 1), and summarize their characteristics into four REE deposit types on the basis of the age, host rock type and mineral associations (Table 1). An integral part of the study was the textural and mineral-chemical comparison of REE, Y, Th, U-rich mineral assemblages in different geological environments.

Table 1. Types of significant REE occurrences in Finland.

| Deposit Examples | Ore-Bearing Rocks | Age(Ga) | Major REE Bearing Minerals |
|--------------------------------------|--|-----------|---|
| Carbonatite rocks | | | |
| Sokli Jammi/ Kaulus | Carbonatites | 0.38–0.36 | Ancylite-(Ce), monazite, bastnäsite, allanite, xenotime-(Y), Sr-apatite, strontianite, barite |
| Korsnäs | Calcsilicate rocks (skarn) next to carbonatite | 1.90–1.83 | Apatite, monazite, Ca-ancylite, bastnäsite, barite, calcite |
| Kortejärvi-Laivajoki | Carbonatites | 1.88–1.85 | Apatite, allanite, chevkinite-(Ce) monazite, bastnäsite, columbite |
| Alkaline rocks | | | |
| Otanmäki and Katajakangas | Alkaline gneiss | 2.30–1.90 | Fergusonite(Y), fergusonite (U), allanite, Ca-REE fluorocarbonates (bastnäsite and synchysite), columbite |
| Tana Belt (Vaulo and Mäkärä) | Arkose gneiss | 3.10–2.60 | Euxenite, columbite, zircon |
| Hydrothermal alteration zones | | | |
| Kuusamo_Uuniniemi | Epigenetic hydrothermal | 1.90–1.80 | Apatite, monazite, allanite euxenite, Fe-columbite, thorite |
| Kuusamo_Honkilehto | Albitite | 2.45–2.44 | Apatite, bastnäsite, ancylite, allanite, chevkinite-(Ce) davidite, uraninite |
| Granitoids/greisen | | | |
| Kovala | Pegmatite in monzogranite | 1.85–1.79 | Monazite, huttonite/thorite, xenotime |
| Kymi granite | Greisen in Rapakivi Granite | 1.64–1.63 | Apatite, monazite, bastnäsite, allanite, xenotime, thorite |

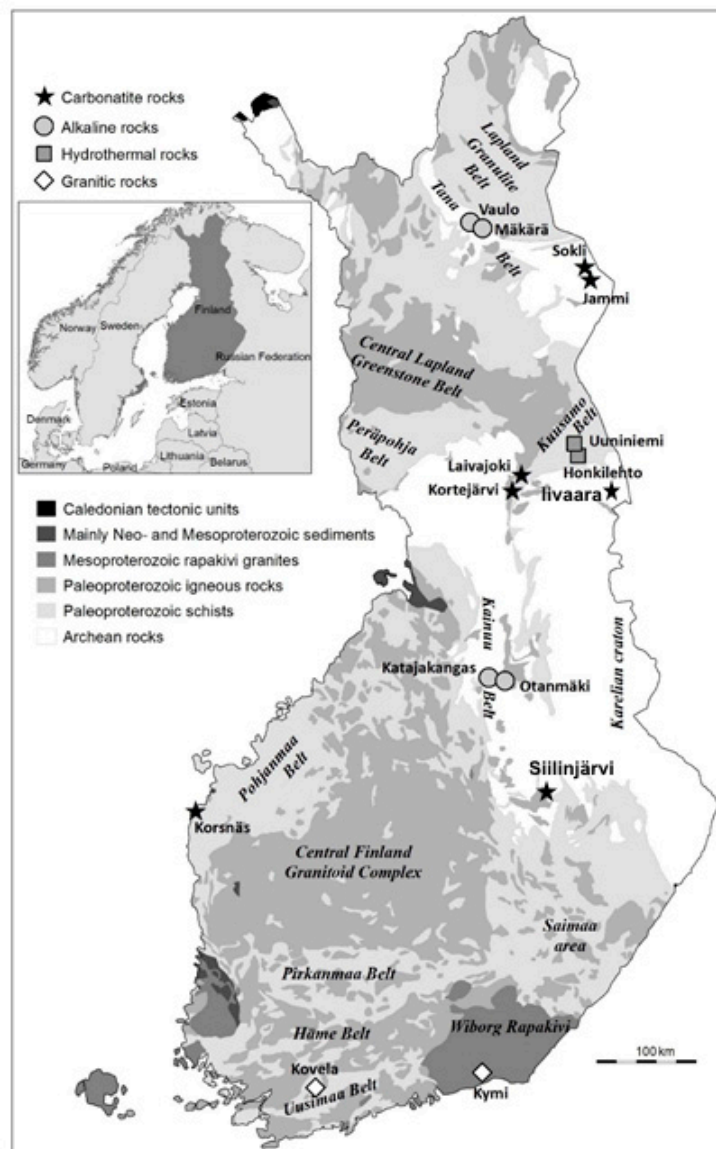


Figure 1. Simplified geological map of Finland with locations of the main REE deposits and occurrences. Modified after Korsman et al. and Nironen et al. [18,19] respectively.

2. Materials and Methods

The first step of this study was the extension of the previous geological, mineralogical, petrological and geochemical databases with new observations on the recently completed new drill cores. On the basis of the results of the revision, drill cores were selected for re-logging and re-sampling for the purpose of detailed petrography and mineralogical studies. Polished thin sections were prepared from representative samples in order to investigate the mineralogical-textural characteristics of REE minerals and their host rocks by transmitted and reflected light polarizing microscopy and by scanning electron microscopy (SEM). For the purpose of high resolution SEM studies, the polished thin sections were carbon coated to a thickness of 25 nm using an EMITECH 960 L evaporation-coating unit. Backscattered electron imaging and qualitative compositional characterization of the samples was performed using an JEOL JSM 5900 LV high-resolution scanning electron microscope (GTK Electron optics and microanalysis Laboratory, Espoo, Finland) fitted with an Oxford Instruments X-MAX large area (50 mm²) silicon drift detector (SDD) energy-dispersive X-ray microanalysis (EDXA) system, run

with Oxford Instruments' INCA v.4 software. SEM analyses were particularly suited to the complexity and very fine grained nature of the mineral assemblages.

Compositions of REE minerals were analyzed using a CAMECA SX100/LKP type electron microprobe equipment (GTK Electron Optics Laboratory). During the analyses, the accelerating voltage was 15 keV with a beam current of 20 nA. The beam diameter was 1 μm in the analyses without fluorine and 5 μm when fluorine was included in the analyzed set of elements. A detailed analytical method is presented in Appendix A and electron probe microanalyzer (EMPA) data are presented in the tables of the Supplementary Material.

3. Geological and Mineralogical Characteristics of Major REE Deposits and Occurrences in Finland

3.1. REE Deposits in Carbonatites

3.1.1. The Jammi and the Kaulus Carbonatite Dikes in the Sokli Complex

The Sokli carbonatite complex (c. 360–380 Ma) in north eastern Finland is a part of the Kola alkaline magmatic province [20], and hosts an unexploited phosphate deposit enriched in REE, Nb, Ta, Zr and U [21,22]. The complex has a concentrically zoned structure that can be divided into two major zones (Figure 2). The inner zone is built up by multiple intrusions of carbonatites and phoscorites whereas the outer zone mainly consists of ultramafic rocks which were largely transformed into carbonate-rich metasomatites by CO_2 -rich fluids derived from the late stage injections of carbonatite melts. The relict minerals and bulk compositions indicate that the ultramafic rocks were mostly pyroxenites [23,24]. The internal zones of carbonatite are surrounded by syenite and a fenite aureoles. The outer boundary of the fenitic zone is up to 2 km away from the central part of the complex. The late stage carbonatite dikes penetrate not only the complex, but also the fenitic aureole and country rocks up to 1.3 km from the contact. The country rocks consist of ultramafic and mafic volcanic units and tonalitic gneiss (Figure 2).

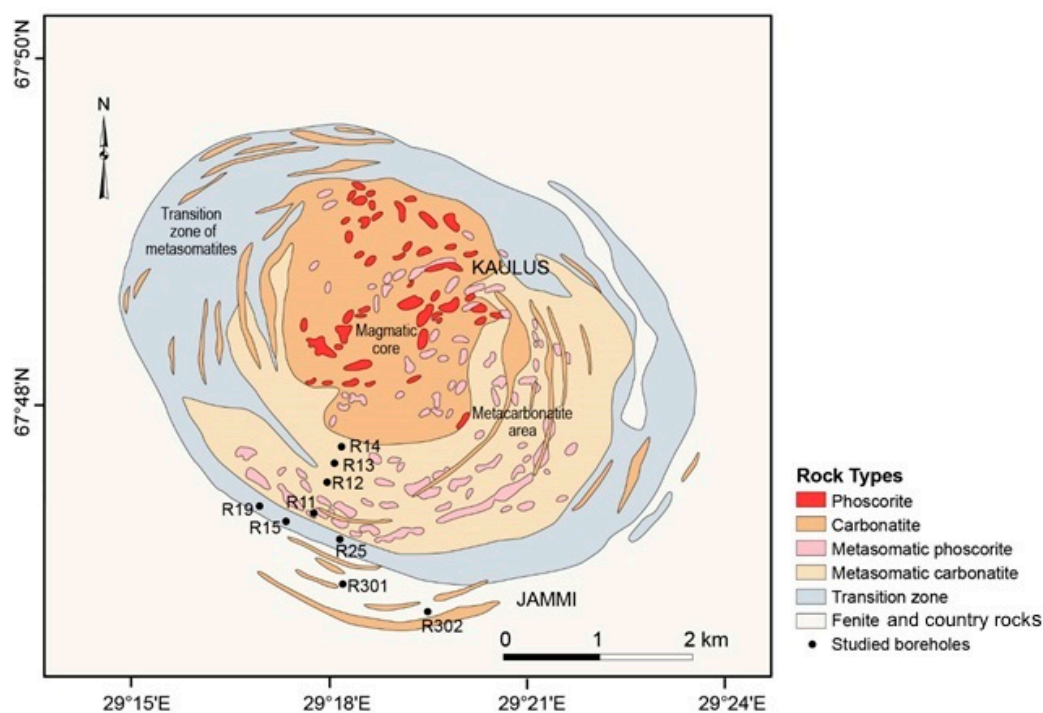


Figure 2. Geological map of the Sokli massif in the northern Finland. Modified after Vartiainen [20].

There is a strong connection between the complexity of fenite textures and associated mineralization due to the enrichment of REE in the intermediate and late stage carbonatite magma generations which produced multiple pulses of fenitizing fluids [21,25]. The presence of brecciated zones within the carbonatite and alkaline complex is the result of an explosive release of fluids and volatiles, thus brecciation indicates development of more evolved magma generations and increased potential of Nb and REE enrichments in the source intrusion [25,26].

Geochemical data from the drill cores R301 and R302 drilled by GTK in 2006 in the Jammi area (Figure 2) show that the carbonatite dikes in the fenitic aureole of the Sokli Complex are enriched in incompatible elements, such as P_2O_5 (19.9 wt % max), Sr (1.9 wt %), Ba (6.8 wt %) and Zn (0.3 wt %). The total REE content of samples are from 0.11 to 1.83 wt %, with dominance of LREE (0.11–1.81 wt % LREE and 0.002–0.041 wt % HREE contents [25]. Similar dikes also occur within the carbonatite intrusion in the Kaulus area (Figure 2). According to the results of whole rock geochemical analyses, most of dikes are varieties of carbonatite ranging from silico-carbonatite to ferro- and calico-carbonatite. Calcio-carbonatite dikes are rich in calcite (15–84 vol %) with subordinate amounts of dolomite, but locally contain up to 50 vol % apatite.

The REE minerals in the carbonatite dikes at Jammi and Kaulus (Figure 2) are usually LREE-rich and their assemblages consist of ancylite-(Ce), monazite-(Ce), bastnäsite-(Ce) and allanite. In the main mass of the Sokli Carbonatite, HREE rich minerals such as xenotime-(Y) and pyrochlore are more common. In general, ancylite is the most widespread REE mineral in the whole complex. This mineral occurs in close association with strontianite, barite and bastnäsite. These minerals commonly form complex intergrowths in the carbonate matrix of dikes, but also fill up veinlets and they can also be found as euhedral crystals in cavities of the carbonatite (Figure 3a).

Ancylite-(Ce) $[CeSr(CO_3)_2(OH) \cdot H_2O]$ from the Jammi carbonatite dyke consists of 31–34 wt % Ce_2O_3 , 11–14.5 wt % La_2O_3 , 8.1–9.3 wt % Nd_2O_3 and 18.2–24 wt % SrO with relatively high Ca (0.5–2.5 wt % CaO) and Th contents (1.8–4.9 wt % ThO_2) whereas Ba has low concentrations (0.5 wt % BaO) (Supplementary Materials Table S1). The atomic proportion of Sr and REE in the formula is close to 1:2, with a small excess of REE.

Monazite-(Ce) $[(Ce,La,Nd,Th)PO_4]$ is the second important REE mineral in the carbonatite dikes of the Sokli complex. This mineral most commonly occurs in the form of microcrystalline, sporadic, and isolated equidimensional crystals in the carbonate matrix. Monazite also often occurs in a round, sunflower-like form. In the centre of latter precipitations, strontium-apatite is often present (Figure 3b,c). The total RE_2O_3 contents are in the range of 40–50 wt % with systematic differences in chemical compositions according to the different stages of monazite crystallization in different assemblages. The monazite crystals have higher in Ce_2O_3 contents (29.5–45.0 wt %) than the sum of La_2O_3 and Nd_2O_3 (e.g., $La_2O_3 = 21.10\text{--}24.66$ wt %, $Nd_2O_3 = 5.81\text{--}7.56$ wt %).

Bastnäsite-(Ce) $[(Ce,La)(CO_3)F]$ has been reported as a relatively common product of alteration of allanite and Sr- or F-apatite [25] in the Sokli complex. Individual crystals of bastnäsite and allanite in the carbonatite dikes appear to be acicular or needle-like and they form either radial accumulations or intricate cross-cutting grids within a variety of minerals such as albite and dolomite (Figure 3d). Allanite-(Ce) $[(Ce,Ca,Y)_2(Al,Fe^{3+})_3(SiO_4)_3(OH)]$ also occurs as both stubby and acicular crystals, generally in contact with bastnäsite and, at some places, with xenotime (Figure 3e). Representative electron-microprobe results of bastnäsite, allanite and xenotime are shown in the Supplementary Materials Table S1. Pyrochlore $[(Na,Ca)_2Nb_2O_6(OH,F)]$ is one of the tantalum/niobium oxides (commonly comprising a U-Ta-rich and Nb-bearing rutile) that typically occurs as a rare, sector-zoned and prismatic crystals with up to 50–100 μm sizes (Figure 3f).

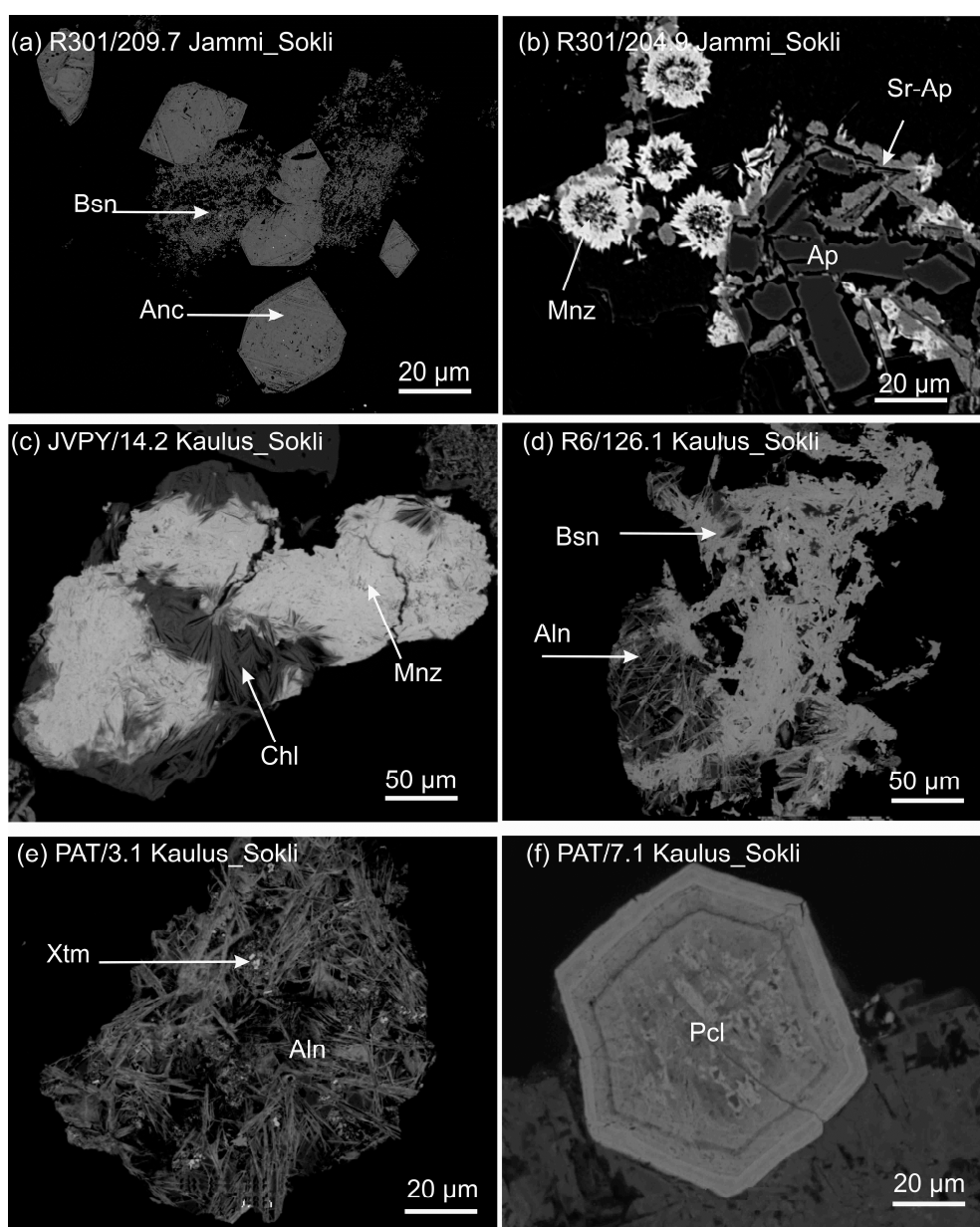


Figure 3. Back-scattered electron images of REE-bearing minerals of Sokli carbonatite; (a) Pseudomorphic hexagonal prisms of ancylite (Anc) and bastnäsite (Bsn) occurring as aggregates with ancylite rims or filling the fracture of minerals; (b) Circular sunflower-like monazite (Mnz) associated with apatite (Ap); (c) Monazite associated with chlorite (Chl); (d,e) Acicular to fibrous crystals of allanite (Aln) associated with bastnäsite (Bsn) and xenotime (Xtm); (f) Hexagonal pyrochlore (Pcl) crystal.

3.1.2. Korsnäs Pb-REE Deposit

The Korsnäs Pb-REE deposit in western Finland was operated by the Outokumpu Oy mining company between 1961 and 1972. The deposit comprises a network of narrow carbonatite veins and dikes in an area of 10 km² and one larger carbonatite dyke (Svartören) that hosts the main ore body measuring 5–30 m in width, up to 1.5 km in length and extending down to a depth of around 350 m (Figure 4). The Korsnäs dyke swarm is hosted by a north-south trending fracture zone dipping to east at an angle of 40–60°. The host rock of the dikes is the c. 1.9 Ga migmatitic biotite paragneiss of the South Ostrobothnian Schist Belt and the carbonatite dikes are dated at c. 1.83 Ga [27]. The average total

REE oxide grade is 0.91 wt % [28]. The ore bodies consist of highly altered intrusive phases, including coarse-grained pegmatite and carbonatite dikes or calcareous scapolite-diopside-barite veins that may contain significant REE grades. The REE contents are correlated with the abundance of apatite (more than 6 wt %) with a slight excess of HREE with respect to presence of monazite and allanite [29,30].

Samples for the current geochemical and mineralogical studies were selected from the drill holes SÖ-66 and SÖ-104 which were drilled by the Geological Survey of Finland in 1955 (Figure 4). The total REE content of samples ranges from 0.7 to 2.2 wt % with LREE dominating the REE budget. The Eu content is high, from 66 to 242 ppm, whereas the Th contents range from 107 to 604 ppm. Ba and Sr are also enriched (3600–3800 ppm and 2200–3400 ppm respectively) mainly in the carbonatite dikes [13,17].

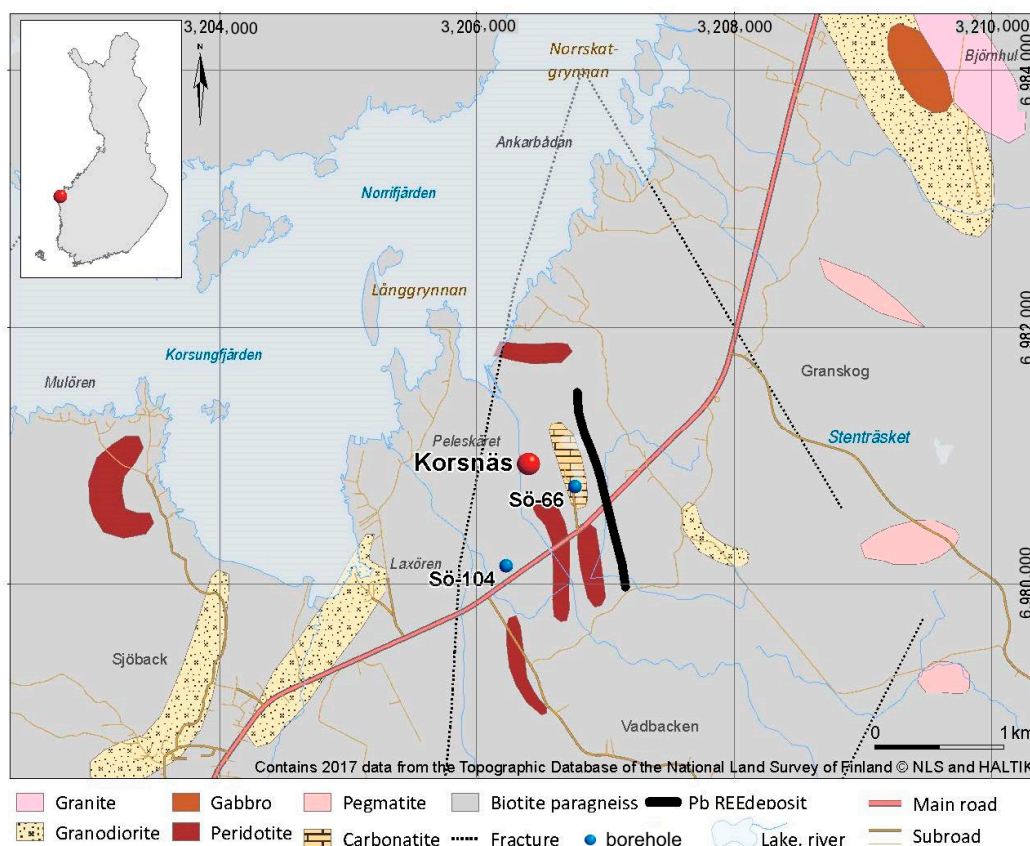


Figure 4. Geological map of the bedrock in the Korsnäs area according to the electronic DigiKp map sheet of the Geological Survey of Finland. Coordinates correspond to Finnish National Coordinate System ETRS-TM35FIN.

The accessory mineral assemblages in the carbonatite dikes of the Korsnäs zone are virtually identical, and include REE-bearing apatite, monazite, bastnäsite, ancylite, britholite, calcite and barite. Representative microprobe analyses of ancylite, bastnäsite and monazite are presented in the Supplementary Materials Table S2. The polycrystalline aggregates of ancylite-(Ce) occurring in some samples as disseminations in the carbonate matrix (Figure 5a) are characterized by a high LREE content: ~45 wt % Ce_2O_3 , ~25 wt % La_2O_3 and ~12 wt % Nd_2O_3 . Ancylite also forms fine-grained aggregates with bastnäsite. Figure 5b shows one example of their typical intergrowths in which bastnäsite cores are overgrown by ancylite. Bastnäsite contains 55.52–59.27 wt % REE_2O_3 , 3.40–5.63 wt % F and 6.31–6.90 wt % CaO. Monazite is the main REE mineral with up to 60 wt % REE_2O_3 . This mineral occurs as small, discrete crystals or as fine-grained inclusions in apatite within the zones of the weathered rocks (Figure 5d–f). Based on the EMPA data (Supplementary Materials Table S2), monazite grains contain an average of 29 ± 1.4 wt % Ce_2O_3 , 11 ± 1.2 wt % La_2O_3 and 8 ± 0.5 wt % Nd_2O_3 , 2 ± 0.5 wt %

Pr_2O_3 with considerable amounts of ThO_2 (6.5 ± 0.5 wt %) and UO_2 (3.2 ± 0.6 wt %). Barite occurs as a secondary mineral, fracture and vug-filling phase together with the REE mineralization (Figure 5e,f). Barite composed mainly of BaO (54.7–62.0 wt %), SO_3 (19.6–33.1 wt %) and SrO (0.4–4.5 wt %). The composition of barite can be seen to be dominated by REE (0.3–18.0 wt % Ce_2O_3) and P (0.1–3.9 wt % P_2O_5), maybe due to partially replaced by various assemblages of REE-Sr-Ba minerals (Supplementary Materials Table S1).

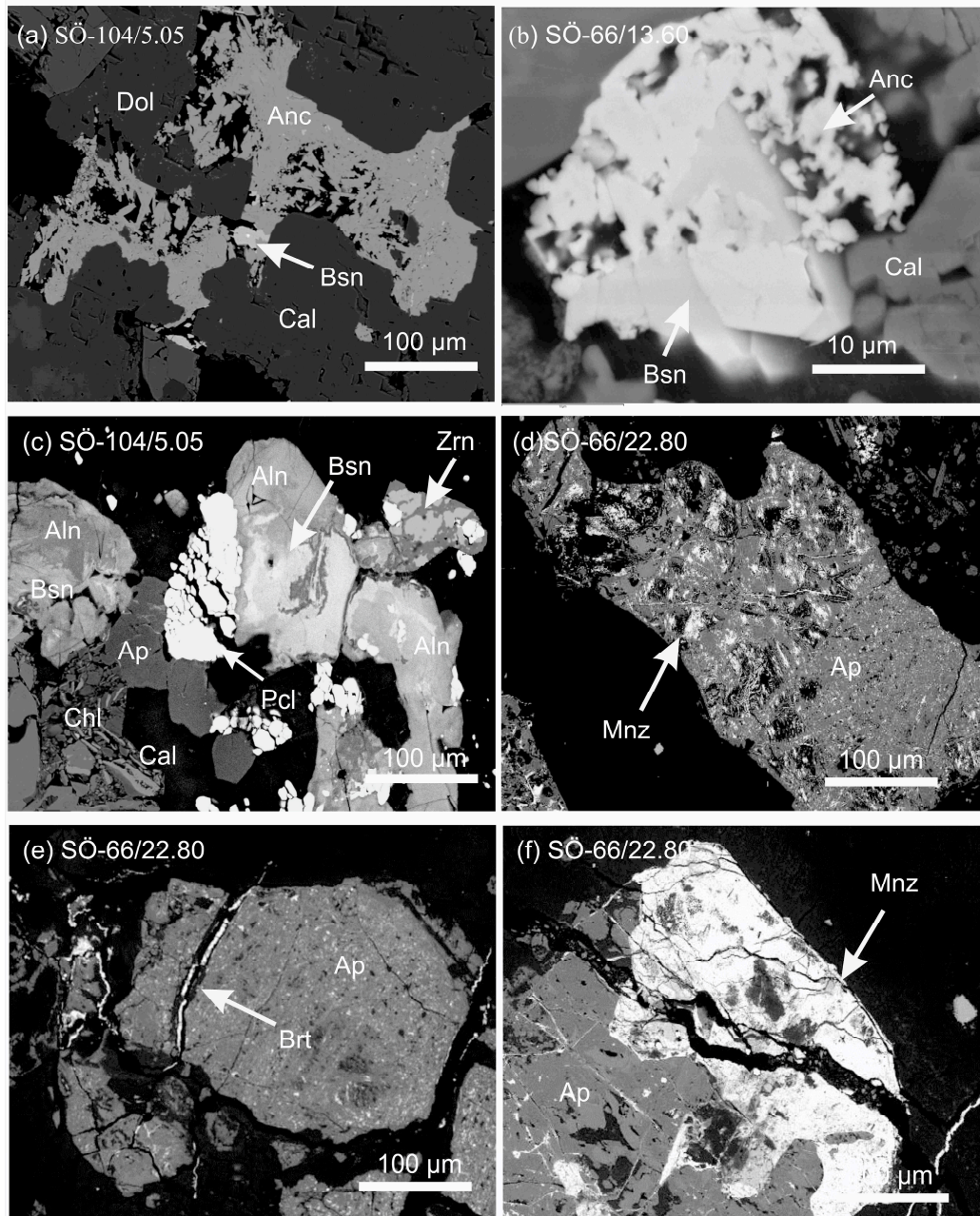


Figure 5. Back-scattered electron images of REE-bearing minerals from the Korsnäs carbonatite; (a) Ancylite (Anc) with carbonate minerals as calcite (Cal) and dolomite (Dol); (b) Overgrowth bastnäsite (Bsn) and ancylite (Anc); (c) Allanite (Aln) and bastnäsite (Bsn) associated with deformed pyrochlore (Pcl) crystals, euhedral apatite (Ap) and zircon (Zrn); (d) Large clusters of monazite grains occur as inclusions within apatite phenocryst; (e) Barite (Brt) filling fractures within apatite grain; (f) Monazite associated with apatite and barite.

3.1.3. Kortejärvi and Laivajoki Carbonatites

The 1.88–1.85 Ga [30] Kortejärvi and Laivajoki carbonatite dikes in the Kuusamo belt, north central Finland (Figures 1 and 6), were emplaced into early Paleoproterozoic mafic volcanic rocks along a crustal-scale fault zone. The Kortejärvi carbonatite dyke is approximately 60 m thick and 2 km long and dips steeply to the east, whereas the Laivajoki carbonatite dyke is about 20 m thick and 4 km long and dips 60° to the southeast [31]. Both dikes consist of calcite-carbonatite and dolomite-carbonatite. The Kortejärvi dyke also contains glimmerite and olivine magnetite rocks, whereas silicocarbonatite and glimmerite occur in the Laivajoki dyke. Total REE contents are 210–1644 ppm and 443–892 ppm in the Laivajoki and in the Kortejärvi carbonatite, respectively [13].

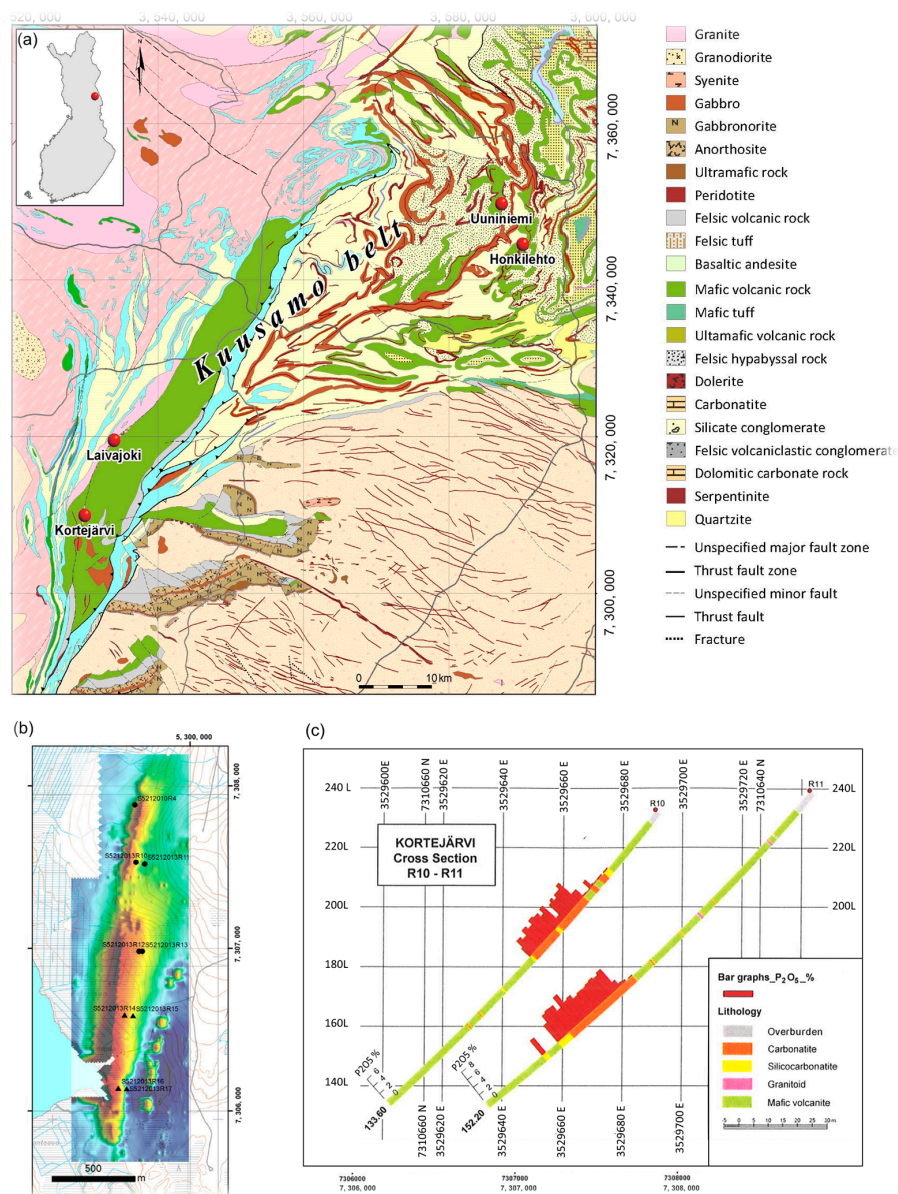


Figure 6. (a) Locations of the Kortejärvi-Laivajoki carbonatite intrusions and metasomatic-hydrothermal REE enrichments at Uniniemi and Honkilehto in the Kuusamo belt; (b) a magnetic ground survey map showing the location of the drill holes; (c) Cross section in Kortejärvi carbonatite showing P₂O₅ contents in drill cores R10 and R11 (modified from [13]). Coordinates correspond to Finnish National Coordinate System ETRS-TM35FIN.

Three samples were selected from the available drill cores of Kortejärvi carbonatite dyke for the purpose of mineralogical studies. The major rock forming minerals are calcite, dolomite and apatite. Apatite is interstitial between calcite and dolomite crystals, and commonly rimmed by overgrowths of monazite (Figure 7a–c). This kind of monazite apatite association is also quite common in carbonatite related deposits. Similar rim of monazite also occurs around calcite and dolomite (Figure 7b). Apatite has 53–54 wt % CaO content without significant concentrations of those trace elements (e.g., REEs, Y, Sr, Th, and U) that may substitute Ca in the crystal lattice. Apatite crystals are very rich in halogens with higher than 2 wt % F and over 1 wt % Cl concentrations (Supplementary Materials Table S3).

The most important REE-bearing accessories are monazite, allanite, synchysite and bastnäsite. These minerals associate with calcite, fluorapatite and quartz in fracture infillings within carbonate minerals and in aggregates of radiating individual crystals with bastnäsite (Figure 7c). Allanite grains are commonly altered into REE fluorcarbonate minerals, most often into bastnäsite (Figure 7c), suggesting to the F-rich nature of overprinting fluids. Bastnäsite forms radial or irregular aggregates of thin tabular crystals with up to ~50 μm sizes in cavities and cracks of altered allanite crystals. Monazite has low (from 0.03 to 3.05 wt %) CaO content with P_2O_5 concentrations between 27.92 and 29.91 wt % (Supplementary Materials Table S3). It contains Ce_2O_3 as the most abundant REE oxide with concentrations ranging from 35.44 to 38.53 wt %, followed by La_2O_3 from 14.43 to 20.98 wt %, and Nd_2O_3 from 9.61 to 13.46 wt %. ThO_2 displays low concentrations, from 0.02 to 1.07 wt %, and it is under the detection limit of microprobe analyses. Allanite-type minerals are characterized by high REE (43.43–47.70 REE_2O_3 wt %), Fe (8.03–11.05 FeO wt %), and Ti (2.93–3.65 TiO_2 wt %) contents, together with low contents of Mn (from 0.07 to 0.13 MnO wt %) and Mg (from 0.66 to 0.93 MgO wt %). The majority of bastnäsite grains in the studied samples are strongly enriched in LREE with approximately 70 wt % total REE. The average Ce_2O_3 is 33.35 wt %, whereas the average La_2O_3 is 19.1 wt % and the average Nd_2O_3 is 8.3 wt %.

Six representative samples of the silicocarbonatite rocks from cores of drillings conducted by the Rautaruukki Corporation in the 1970s were chosen for mineralogical studies from the Laivajoki dyke. Mineral assemblages in the samples consist primarily of quartz, calcite, dolomite, plagioclase, biotite and iron oxide minerals. Allanite and chevkinite are the most abundant REE-bearing minerals. Allanite occurs in the form of coarse-grained aggregates associated with silicate and iron oxide minerals. Allanite also contains inclusions of magnetite and chevkinite (Figure 7d). The grain size of allanite varies between 300 μm \times 500 μm and 1000 μm (Figure 7e). Many crystals display a network of fractures with narrow strips of epidote (Figure 7d,e). Chevkinite fills fractures in iron oxide minerals and titanite (Figure 7f). REE-rich fluorcarbonate minerals (bastnäsite and synchysite) are commonly associated with each other but bastnäsite is more abundant in most of the studied samples. Bastnäsite also occurs as tiny anhedral inclusions up to 20 μm across in synchysite. Synchysite also forms radial or irregular aggregates of thin tabular crystals with up to ~50 μm sizes in cavities and cracks of altered allanite crystals, or in association with calcite, dolomite and Ti-bearing phases in some places (Figure 7f). The secondary carbonate minerals (mainly synchysite and bastnäsite) replace substantial parts of former allanite crystals (Figure 7f).

Results of electron microprobe analyses in polycrystalline allanite (Aln) grains from Laivajoki are given in Supplementary Materials Table S3. Allanite is characterized by relatively uniform composition with REE_2O_3 contents between 24.67 and 27.09 wt %, small Y contents (0.08–0.13 wt % Y_2O_3), and from 11.05 to 12.36 wt % Al_2O_3 , from 11.26 to 13.52 wt % FeO total, from 10.41 to 12.22 wt % CaO and from 3.98 to 4.99 wt % MgO contents. ThO_2 and MnO_2 contents are very small, not exceeding 0.5 wt %. In places, a phase with intermediate allanite-epidote composition, showing elevated Al (~20 wt % Al_2O_3), Ca (~15 wt % CaO) and smaller Fe (~12 wt % $\text{FeO}_{\text{total}}$) and (REE,Y) $_2\text{O}_3$ contents of 15 wt % were also found in fractures of allanite.

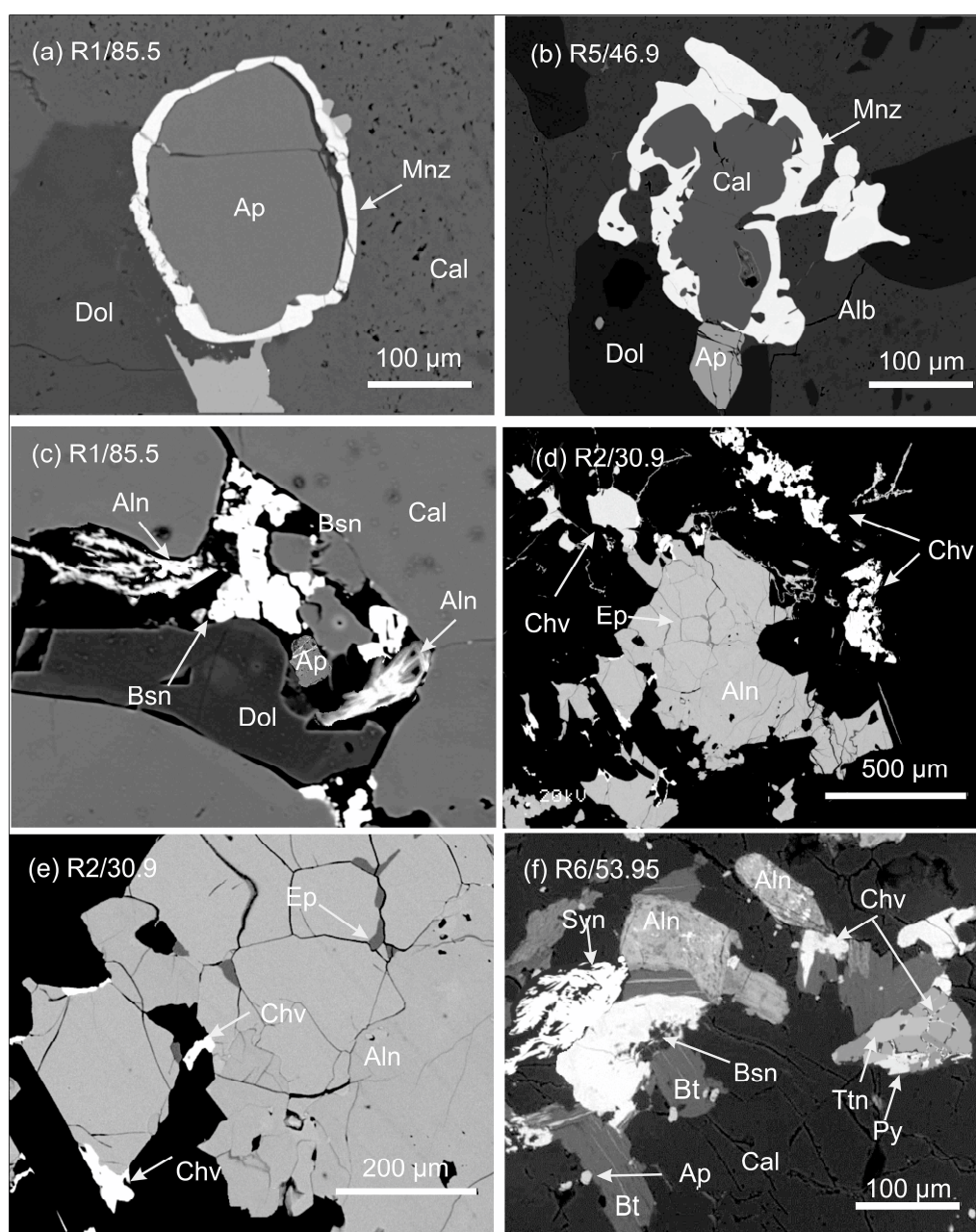


Figure 7. Back-scattered electron (BSE) images of REE-minerals from Kortejärvi and Laivajoki carbonatite samples; (a,b) Monazite (Mnz) associated with apatite (Ap), calcite (Cal), dolomite (Dol) and albite (Alb); (c) Bastnäsite (Bsn) and acicular allanite (Aln) in association with fluorocarbonate minerals; (d,e) Large allanite crystal within fractures filled by epidote (Ep), and the rim of allanite is replaced by secondary chevkinite (Chv; bright zones); (f) Acicular synchysite (Syn), chevkinite (Chv) and bastnäsite in association with allanite, biotite (Bt) and calcite. Chevnikite also fills fractures in titanite (Ttn) and pyrite (Py).

In the samples from the Laivajoki carbonatite dyke, the majority of bastnäsite grains are strongly enriched in LREE (from 67.29 to 77.98 wt % REE₂O₃) with up to 33 wt % Ce₂O₃, 12 wt % La₂O₃, 18 wt % Nd₂O₃, and smaller contents of the remaining REE. Fluorine is the dominant anion (from 3.1 to 4.7 wt % F) and is partly substituted by hydroxyl. Synchysite-(Ce) [Ca(REE)(CO₃)₂F] reveals a significantly higher Ca content (from 11.74 to 17.32 wt % CaO) in comparison to bastnäsite but LREE still predominate in the composition with Ce³⁺ being the dominant REE cation (from 23.15 to

30.94 wt % Ce_2O_3). The F content shows small variation from 3.1 to 4.8 wt % and the ThO_2 content is just over 1 wt %.

Chevkinite-(Ce) has the general formula of $\text{A}_4\text{BC}_2\text{D}_2(\text{Si}_2\text{O}_7)_2\text{O}_8$, where the predominant cations in each site are: A = Ca, REE, Th; B = Fe^{2+} ; C = Fe^{2+} , Fe^{3+} , Ti; and D = Ti. Oxide totals of microprobe analyses from this phase are rather low (from 94.9 to 96.3 wt %) presumably due to presenting total Fe as Fe^{2+} (see below), and perhaps due to secondary hydration during metamictization. Chevkinite from Laivajoki has notably low Ca contents (~1 wt % CaO) and correspondingly high REE contents (48.62–50.74 wt % REE_2O_3). Thorium contents are very low (<0.10 wt % ThO_2). Thus, REE occupy more than 98% of the A-site. Divalent Fe is the dominant cation at the C-site, with values of FeO concentrations ranging from 9.27 to 9.48 wt %, whilst MgO values are slightly elevated (from 1.38 to 2.13 wt %). The SiO_2 , TiO_2 and Ce_2O_3 are the main oxides with 18.19–19.52 wt % SiO_2 , 15.26–15.74 wt % TiO_2 and 26.56–28.68 wt % Ce_2O_3 concentrations.

3.2. REE Deposits Related to Alkaline Intrusions

3.2.1. The Otanmäki Katajakangas Nb-REE Deposit

The Otanmäki area consists mainly of Archean granitic gneisses intruded by alkali-granite and gabbro-anorthosite of c. 2.05 Ga age (Figure 8) [32–34]. The gabbro-anorthosite intrusions host Fe-Ti-V deposits which were mined from 1950's to 1980's by the Otanmäki Oy mining company. In total, 30 Mt of ore grading of 32–34% Fe, 5.5–7.6% Ti and 0.26% V was mined [35]. The processing plant in Otanmäki produced 7.6 Mt magnetite, 3.8 Mt ilmenite and 0.2 Mt sulphur concentrates, as well as 55,454 t vanadium pentoxide [36]. The alkaline gneiss contains 0.7–1.5 wt % Zr and 0.1–0.2 wt % Th [37].

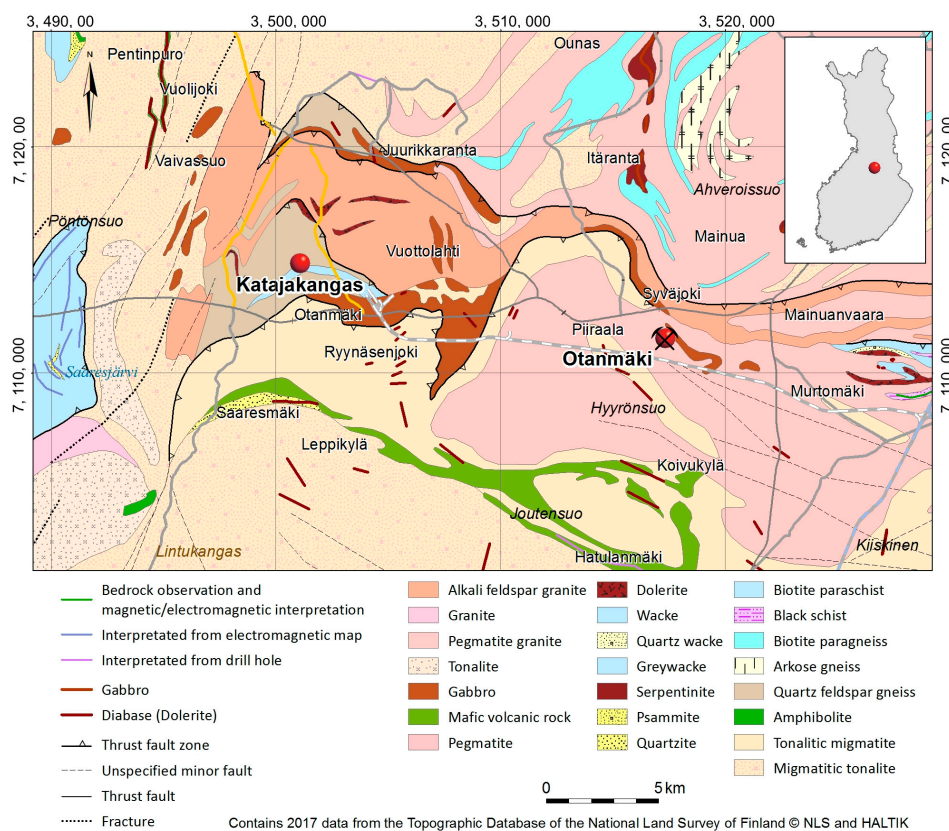


Figure 8. Geology of the Katajakangas and Otanmäki area on the basis of the electronic DigiKP map available at the Geological Survey of Finland. Coordinates correspond to the Finnish National Coordinate System ETRS-TM35FIN.

To the west of the old Otanmäki mine, the Nb-REE mineralisation at Katajakangas occurs in narrow lenses or layers with a few metres width only (Figure 8). These ore bodies are mostly composed of pervasively sheared and foliated, fine-grained, reddish-grey quartz-feldspar gneiss with riebeckite and alkaline pyroxene with some hydrothermal veins. The zones with Nb-REE mineralization in the alkaline gneiss contain high concentrations of Nb, Zr, Y, Th and REE, with an estimated Nb + Y + REE resource of 0.46 Mt at 2.4 wt % RE₂O₃, 0.31 wt % Y₂O₃ and 0.76 wt % Nb₂O₅ contents [7].

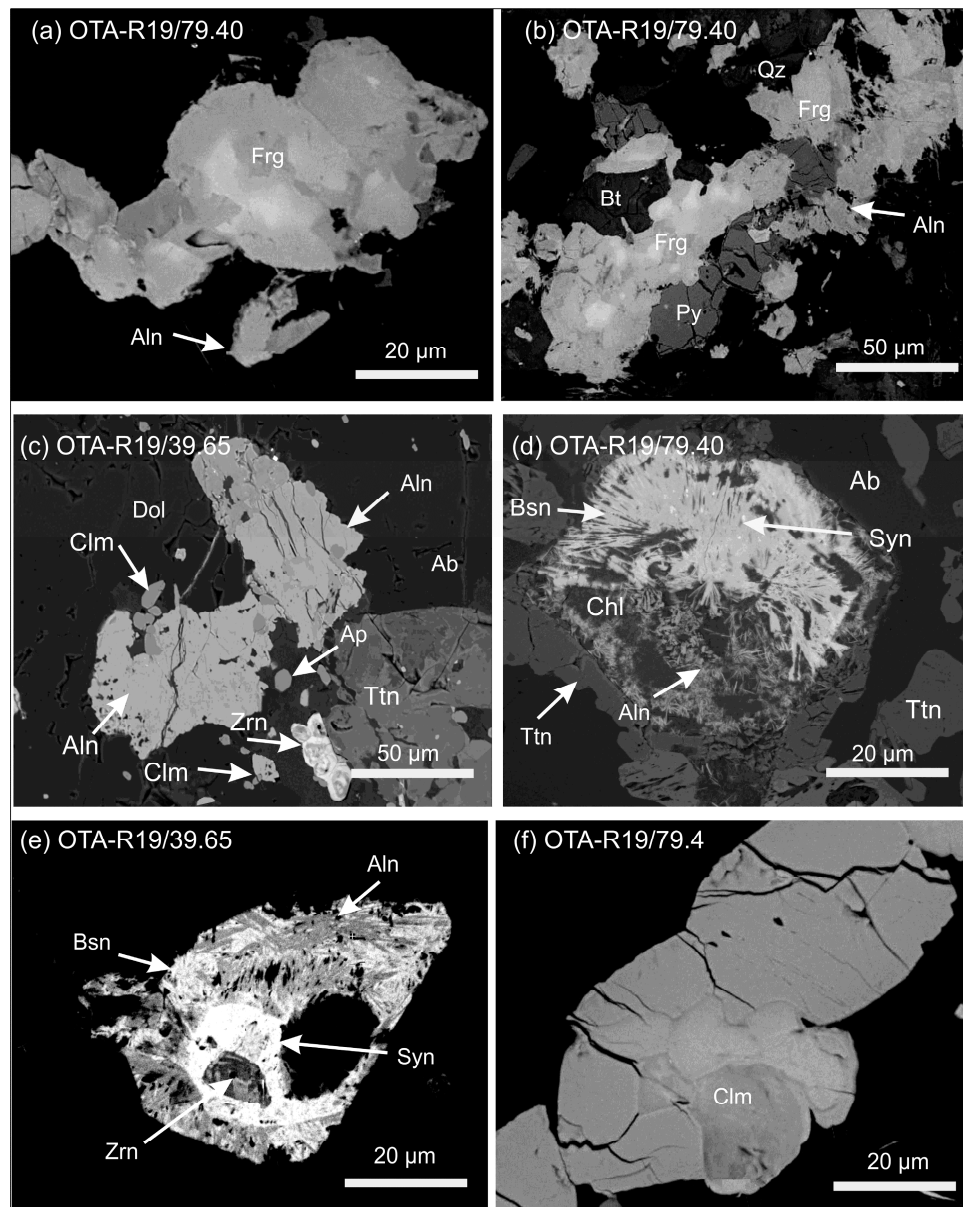


Figure 9. Back-scattered electron images REE-bearing minerals in Otanmäki alkaline granitic samples; (a,b) Fergusonite (Frg) in association with allanite (Aln), biotite (Bt) and pyrite (Py), fergusonite shows mostly patchy zoning with the brightest areas having high U and Th; (c) Primary magmatic allanite (Aln) associated with albite (Ab), biotite (Bt), quartz (Qz), zircon (Zrn), columbite (Clm), apatite (Ap) and titanite (Ttn); (d,e) Aggregates of thin platy crystals of REE carbonate minerals, mainly synchysite (Syn) and bastnäsite (Bsn) in association with allanite (Aln) and chlorite (Chl); (f) Columbite (Clm) as elongate to subhedral shows simple core-rim zoning with U content.

Representative EPMA analyses of the REE-bearing minerals from the Otanmäki-Katajakangas deposit are listed in the Supplementary Materials Table S4. Fergusonite and columbite are the major host for Nb, Th, U and Y, whereas REE is mainly hosted by allanite. Fergusonite-(Y) [YNbO₄] occurs commonly as rounded to irregular discrete crystals varying in size from 100 µm up to more than 500 µm, in associations with allanite, columbite and zircon. Fergusonite is chemically heterogeneous: many crystals display growth zoning with enrichments in U and Th in the cores of crystals (Figure 9a,b). The bright domains on SEM images of these cores are characterized by high content of U (up to 9.5 wt % UO₂), Th (up to 3.1 wt % ThO₂), Y (up to 26 wt % Y₂O₃) and Nb (46.3 wt % Nb₂O₅) (Supplementary Materials Table S4). Textures observed in SEM and EPMA data suggest to the presence of sub-micrometre intergrowths between fergusonite and allanite in most of the studied samples (Figure 9a,b). They are interpreted as early magmatic REE phases. Columbite (Fe,Mn) (Nb,Ta)₂O₆ is the most common niobium-bearing mineral in many of the studied samples. Columbite occurs in the form of irregular-sub round micro phenocrysts with up to ~50 µm sizes in associations with allanite (Figure 9c). Columbite is also present as elongated (250 µm), subhedral to euhedral crystals, which are commonly intergrown with euhedral to anhedral rutile. Columbite and rutile grains are dispersed throughout the matrix of the host rock. The columbite crystals are typically poorly zoned but some parts of the crystals are usually richer in uranium (Figure 9f).

The primary magmatic allanite forms euhedral to subhedral crystals, ~100 to ~300 µm across. It is associated with albite, biotite, quartz, zircon, fluorapatite, and titanite (Figure 9c). Allanite crystals are also partly to fully replace and overgrown by secondary REE carbonates (bastnäsite and synchysite). The Katajakangas allanite has a total REE-content between 23.6 and 55.7 wt % (average 39.6 wt %). Cerium (Ce) is dominant (with average Ce₂O₃ content of 20.7 wt %), followed by Nd (10.7 wt %) and La (7.7 wt %). Concentrations of HREE are commonly below the detection limit of the electron microprobe (Supplementary Materials Table S4). The allanite- bastnäsite-synchysite association form aggregates with more or less hexagonal outlines within the surrounding matrix (Figure 9d). The aggregates consist of radiating individual crystals.

In the hydrothermal veins, synchysite and bastnäsite form well-developed fibrous crystals and aggregates of radiating acicular crystals. The REE-carbonates replace and/or encompass allanite crystals in these veins (Figure 9e).

3.2.2. The Mäkärä Vaulo Area in the Tana Belt

The Tana Belt is located on the southern side of the Lapland Granulite Belt in northern Finland (Figure 1). It is characterized by prominent REE anomalies in till, but lithogeochemical data for various types of rocks also display enrichments in REE [38–41]. High La and Y concentrations in both till and arkose gneisses of the bedrock occur in an elongated, 200 × 200 km² area (Figure 10).

The Mäkärä region within the Tana Belt consists of Archean gneiss (3.1–2.6 Ga) and Paleoproterozoic supracrustal rocks (2.3–2.0 Ga), which were thrust together with the Lapland Granulite Belt onto the Central Lapland Greenstone Belt at c. 1.9 Ga during the Svecofennian orogeny [42–44]. The bedrock of the study area is poorly exposed, and largely covered by saprolite, weathered regolith and Quaternary till with variable thicknesses, as well as with dense vegetation. This area is characterized by Au and REE anomalies in regional till and bedrock samples. Au anomalies can be related to occurrences of hydrothermal hematite-pyrite-quartz veins, whereas weathering of arkose gneiss has played a role in the formation of the REE-bearing kaolinitic saprolite. The REE enrichment in kaolinitic saprolite ranges from 0.04 to 0.1 wt % REE₂O₃, with LREE/HREE ratio of 2.7 to 15 in the kaolinitic saprolite sediment samples.

The arkose gneiss is mainly composed of quartz, K-feldspar, plagioclase, amphibole and mica (muscovite and biotite) phenocryst embedded in fine-grained groundmass. Lamprophyre dikes of 1775 ± 10 Ma [44] intrude the gneissic rocks at Mäkärä. The dikes are mainly composed of plagioclases, amphiboles, biotite, K-feldspars. Remnants/fragments of lamprophyre also occur in the kaolinitic saprolite. The average total REE content of dikes is 0.05 wt % (max 0.1 wt %).

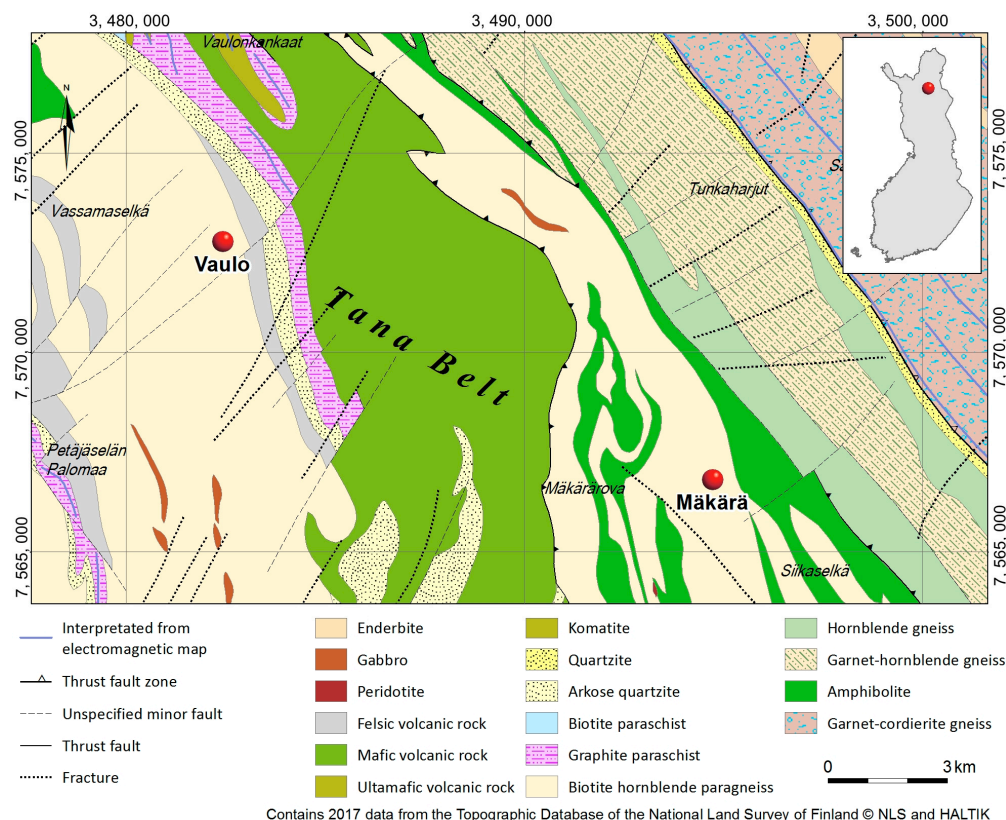


Figure 10. Geological map of the Tana belt in the area of the REE mineralization at Mäkärä and Vaulo. Modified from Salmirinne et al. [38].

Detailed electron-microprobe studies of the arkose gneisses from the Tana Belt revealed extensive sub solidus alteration of primary magmatic allanite to ferriallanite. Moreover, the alteration of ferriallanite resulted in development of complex pseudomorphs and overgrowths containing mainly REE carbonate phases such as synchysite and bastnäsite. Allanite and REE carbonate phases often occur as large anhedral and spheroidal aggregates with up to 200 μm in diameter (Figure 11a–c). Occasionally, these aggregates also fill up vugs. Ferriallanite is often altered to allanite in the rims and to bastnäsite in the centres of the aggregates (Figure 11a–c). Allanite does not show significant zoning by SEM imaging but contains REE-rich rims due to sub-micron sized intergrowths with allanite plus a bastnäsite-type mineral phase. At some places, the secondary carbonate minerals (mainly synchysite) occur in cavities of feldspar and in association with monazite and apatite (Figure 11e).

In the lamprophyre dikes, enrichments of REE are hosted by apatite, allanite, bastnäsite, cerite and xenotime. Rutile contains inclusions of xenotime and iron oxides. Allanite crystals are partly or fully replaced and overgrown by secondary minerals, mainly REE carbonate phases (bastnäsite and synchysite), chlorite, albite, quartz, and more rarely by xenotime, titanite and apatite (Figure 11a–d). Chemical compositions of selected allanite and associated accessory minerals from the lamprophyre dikes in the Mäkärä are presented in the Supplementary Materials Table S5. The oxide totals are in the range 96 to 99 wt %. Part of the short fall can be attributed to calculation of the total iron as FeO. The Ca content ranges between 0.89 and 6.17 wt % CaO and the sum of Y + REE varies from 21.44 to 55.16 wt % with the dominance of Ce (11.38–47.37 wt % Ce_2O_3). The concentration of Th in allanite ranges from 0.020 to 0.80 wt % ThO_2 and usually predominates over U (0.17 wt % UO_2). Generally, M sites of allanite are dominated by Al (14.37–15.83 wt % Al_2O_3) and Fe (8.79–15.16 wt % FeO). The Mg contents (0.12–2.46 wt % MgO) as well as the Si and F concentrations (19.36–31.24 wt % and 0.23–1.10 wt %, respectively) together with the high-end of Fe contents (up to 15.16 wt % FeO) can be attributed to the presence of significant amount of ferriallanite molecule in the composition of allanite. The bastnäsite

compositions in lamprophyre dikes show dominance of light REE (LREE; La to Nd) over other REE, with $Ce > La > Nd > Pr$ abundances, and 33.5 to 38.5 wt % Ce_2O_3 , while calcium reaches only around 1.3 to 2.9 wt % CaO (Supplementary Materials Table S5). Synchronite reveals a significantly higher Ca content (5.62 to 9.14 wt % CaO) in comparison to bastnäsite. Again, LREE predominates here, with Ce^{3+} the dominant REE cation (21.79 to 30.67 wt % Ce_2O_3). The F content of bastnäsite is highly variable (from 3.40 to 6.36 wt % F) whereas it is ranging between 0.62 and 1.26 wt % F in synchronite.

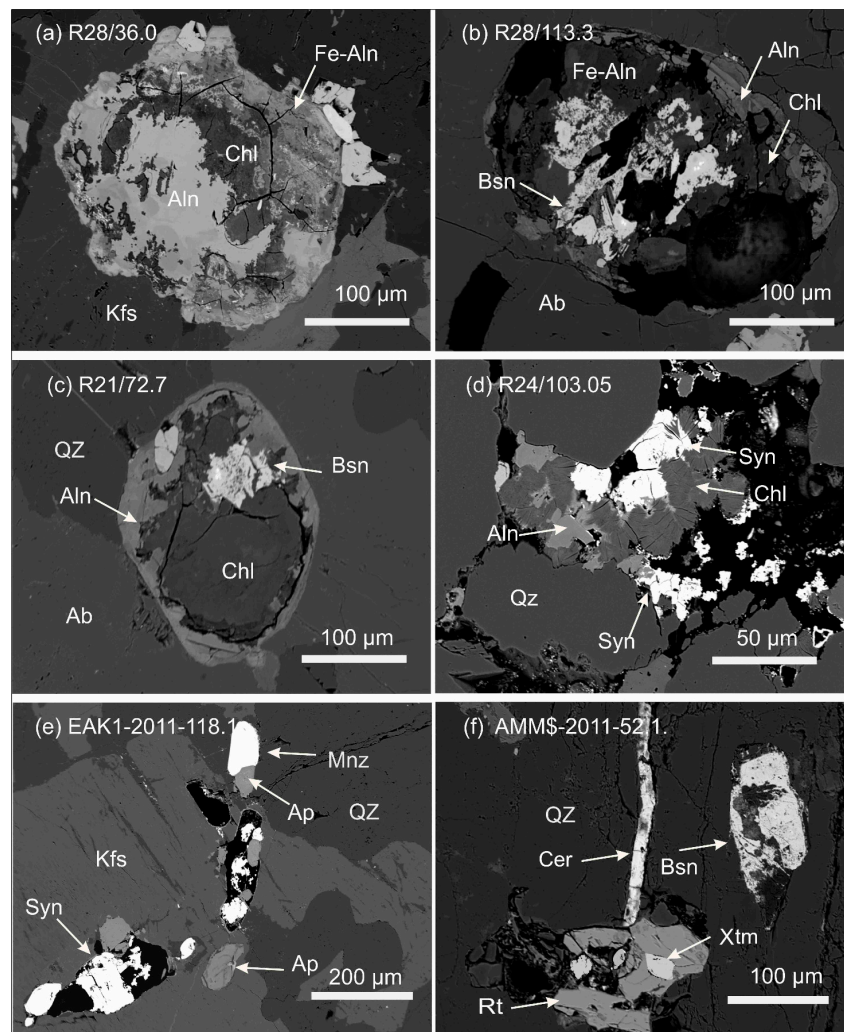


Figure 11. Back-scattered electron images REE-bearing minerals from arkose gneiss of Tana Belt; (a–d) Primary magmatic allanite (Aln) to ferriallanite (Fe-Aln) crystals in association with quartz (Qz), K-feldspar (Kfs), fluorapatite (Ap) and chlorite (Chl) and partly replaced by an assemblage of secondary REE carbonates bastnäsite (Bsn) and synchronite (Syn); (e) Synchronite filling within feldspar and in association with monazite and apatite; (f) Cerite (Cer) fills a small fractures in quartz and albite, and it is in contact with bastnäsite, xenotime (Xtm) and rutile (Rt).

Transformation of allanite to secondary REE carbonate minerals (mainly bastnäsite and synchronite) has been described in numerous cases in various magmatic and metamorphic rocks e.g., [45–49]. However, such alteration of allanite is usually associated with clay minerals (kaolinite, montmorillonite), and also with thorite, fluorite, and magnetite without carbonate minerals in some cases [45,50]. In contrast, allanite in the samples from the Tana Belt was replaced mainly by bastnäsite and synchronite, and rarely also by ferriallanite and chlorite. This type of alteration of allanite suggest to highly alkaline and oxidizing nature of the overprinting fluids [51–54].

Cerite [$\text{Ce}_9\text{Fe}^{3+}(\text{SiO}_4)_6(\text{SiO}_3)(\text{OH})_4$] occurs as fine-grained crystals filling fracture-veins in quartz and albite (50 μm in length and 5–15 μm in width) as seen in the studied lamprophyre dikes (Figure 11f). Cerite is strongly enriched in the LREE and also contains relatively low concentrations of Y and HREE (Supplementary Materials Table S5). The sum of the oxides of La, Ce, Pr, Nd, Sm, Gd, Dy and Y ranges from 71.15 to 81.60 wt %. Cerium-oxide contents are from 67.79 to 77.49 wt%. Cerite also contains from 12.19 to 17.86 wt % SiO_2 , from 1.18 to 2.53 wt % Al_2O_3 , from 0.02 to 2.41 wt % FeO and minor amounts of Ca (0.06–0.39 wt % CaO). Fluorine is invariably present in concentrations ranging from 1.21 to 1.73 wt %. Analytical totals between 94.3 and 99.6 wt % suggest the presence of minor amount of H_2O and other elements below their detection limits.

A few disseminated anhedral xenotime grains (diameter = 15 \times 40 μm and 20 \times 25 μm) have also been found in the lamprophyre dikes of the Mäkärä area. Xenotime also forms inclusions within ilmenite and surrounded by quartz and K-feldspar (Figure 11f). Xenotime [YPO_4] grains contain significant amounts of Y_2O_3 (41.08–47.33 wt %) and extremely high HREE concentration. The Gd_2O_3 contents are up to 4.5 wt % and the Dy_2O_3 content are up to 4.8 wt %.

3.3. Hydrothermal REE Deposits

3.3.1. Uuniemi (Kuusamo Belt)

The Kuusamo schist belt (KSB) is a fold and thrust belt which is considered as a part of the Central Lapland greenstone belt, the most significant Paleoproterozoic orogenic gold province in northern Europe. The KSB consists of an epiclastic-volcanic sequence deposited during multiple rifting events affecting the Archean basement between 2.4 and 2.0 Ga. The lithological units (Figure 6) were metamorphosed and folded during the Svecofennian orogeny (1.9–1.8 Ga). Syenite and carbonatite dikes with strong albitization are widespread in the KSB. Albitization are related to late magmatic and metamorphic hydrothermal processes [55–58].

The zone of REE enrichment at Uuniemi is composed of metasediments, syenite and metasomatic carbonatite dikes [57], which were subjected to intense albitization, Fe-metasomatism, carbonatization and brecciation. The metasomatic carbonatite dyke sampled in outcrops contains 2.8 wt % P_2O_5 , 0.43 wt % REE_2O_3 and 256 ppm Nb. In albitite and albite carbonate rocks, the average total REE content is 0.1 wt % [13]. The albite carbonate rock samples are composed of sodic plagioclase with minor carbonate (calcite and dolomite), quartz and mica (biotite), but are also highly enriched with apatite and REE minerals such as monazite, allanite, euxenite, Fe-columbite and thorite.

Monazite in the albite carbonate rocks (albitite) mostly occurs as grains in composite mineral inclusions in apatite. In such inclusions, the irregular shaped monazite grains are typically 5–20 μm large and occupy 50–70 wt % of the total volume of the inclusions (Figure 12a). Monazite also occurs as relatively large (50–150 μm), oval or anhedral individual grains that are strongly porous and fractured in the matrix of the rock (Figure 12b). Monazite contains much more, ~66 wt % total REE_2O_3 compared to allanite (20.4 wt %), and lower Th and Ca contents (0.22 wt % ThO_2 and 0.33 wt % CaO).

Euxenite occurs as subhedral to anhedral, commonly 200–400 μm large, but occasionally up to 500 μm large grains, (Figure 12c). Electron-microprobe analyses (Supplementary Materials Table S6) of euxenite grains show lower amounts of total REE (from 0.96 to 1.21 wt % REE_2O_3) and higher amounts Nb (36.10–37.56 wt % Nb_2O_5), Y (19.49–19.93 wt % Y_2O_3), and Ca (4.16–4.25 wt % CaO), compared with analyses of monazite and bastnäsite. Small amounts of W (2.50–3.61 wt % WO_3) and U (4.15–4.62 wt % UO_2) and trace amounts of Th (0.49–0.63 wt % ThO_2) were also detected. Thorite commonly occur not only as isolated grains but also as inclusions within monazite and apatite. Thorite is characterized by large agglomerations of anhedral to round crystals with up to 200 μm in diameter (Figure 12d). In addition to $\text{ThO}_2 = 53.19$ – 64.05 wt %, thorite contains 16.02–17.57 wt %, SiO_2 , 4.32–16.38 wt % FeO and 2.94–3.06 wt % UO_2 with some Ce_2O_3 , Y_2O_3 , PbO and P_2O_5 . Ferrocolumbite [(Fe,Mn)(Nb,Ta) $_2\text{O}_6$] crystals that occur in the metasomatic carbonatite dikes of Uuniemi in the form of subhedral to anhedral crystals and range in size from 50 to 200 μm (Figure 12d). The major oxides

in ferrocolumbite are FeO (19.36 wt %) and MnO (1.68 wt %) at the A sites of the crystal structure, whereas Nb₂O₅ (67.26 wt %) and Ta₂O₅ (1.73 wt %) occupies the B-sites. Also, minor amounts of Ti, Th, U, Y and LREE were observed as substitutions (Figure 12d). Apatite occurs as discrete subhedral grains in association with calcite and dolomite. Davidite and rutile are the principal opaque minerals. Davidite is present as large (up to 2 mm in diameter) zoned grains (Figure 12e).

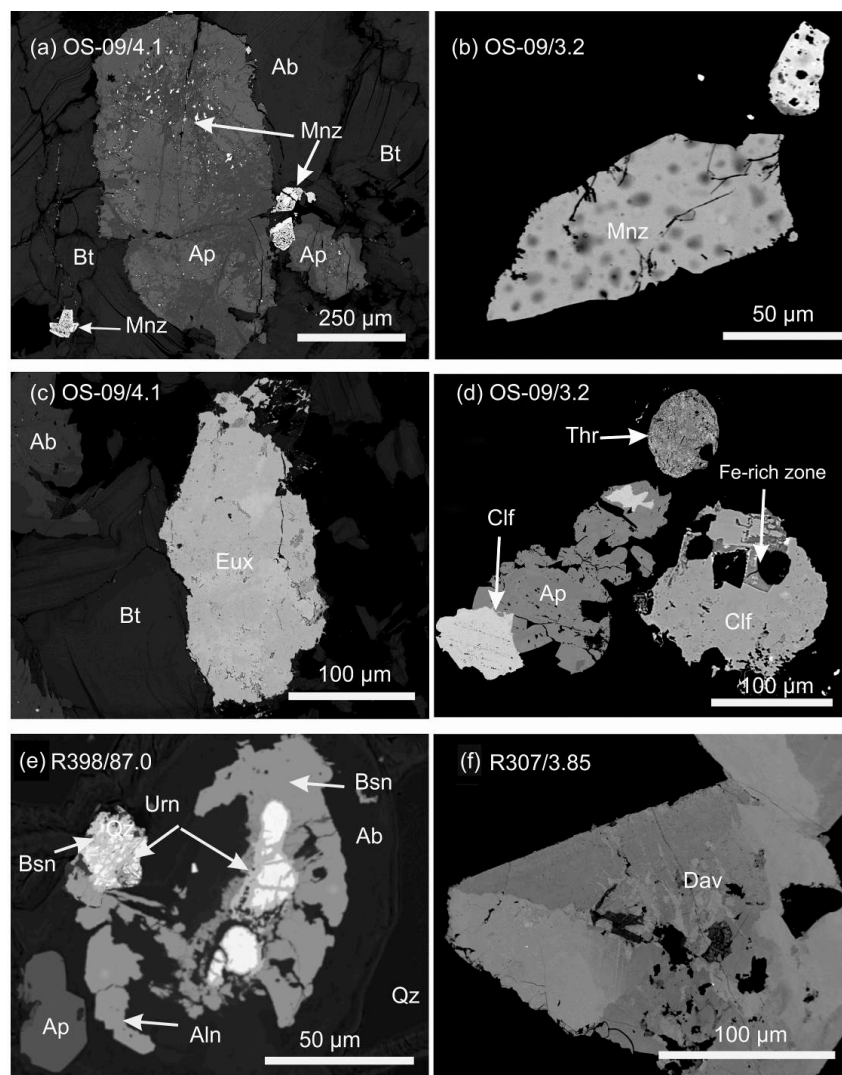


Figure 12. Back-scattered electron images REE-bearing minerals in Kuusamo Belt; (a) Monazite (Mnz) as inclusions within apatite (Ap); (b) Porous monazite; (c) Euxenite (Eux) in association with albite (Ab) and biotite (Bt); (d) Sub rounded Fe-columbite (Clf) associated with apatite (Ap) and thorite (Thr); (e) Uraninite (Urn) grains surrounded by halos of bastnäsite (Bsn) and allanite (Aln); (f) Crystalline to partially damaged davidite (Dav), a member of the crichtonite mineral group and also showing patchy chemical zoning.

3.3.2. Honkilehto (Kuusamo Belt)

The hydrothermal Au-Co-Cu-U-REE occurrence at Honkilehto in the central part of KSB is hosted by albitised, carbonatised and sulphidised sericite quartzite [57], which are intruded by numerous sills of albite diabase and by some minor metasomatic carbonatite dikes [59]. The carbonatite dikes are characterized by high content of P (2.8 wt % P₂O₅) and REE (0.45 wt % total REE₂O₃) and host several REE-bearing minerals such as monazite-(Ce), allanite-(Ce), ancylite-(Ce), bastnäsite-(Ce) and xenotime-(Y). The albite diabase dikes are characterized by high content of U-rich minerals (uraninite,

Davidite), all of which are associated with bastnäsite and allanite [27]. Coexisting bastnäsite and uraninite with up to 100 and 50 μm in size, respectively (Figure 12e), occur as accessory minerals in the host albitised rocks. Uraninite is partly or wholly replaced by bastnäsite and allanite. Bastnäsite is furthermore common in fractures, indicating that it is a paragenetically late mineral (Figure 12e). The pristine parts of the uraninite grains (Supplementary Materials Table S6) contain 71.8–77.5 wt % UO_2 and the Pb content varies from 1.3 to 15.8 wt % PbO. Concentrations of Si are from 0.03 to 6.1 wt % SiO_2 , and the Fe content is from 0.5 to 2.5 wt % FeO. The Y_2O_3 and REE_2O_3 are from 0.5 to 5.5 wt % and from 0.05 to 4.5 wt %, respectively.

Details of REE mineralogy were checked in two drill core samples of albitised and carbonatised sericite-quartzite at Honkilehto. These samples are composed mainly of albite, calcite, biotite, quartz and sericite. Apatite occurs as discrete subhedral grains in association with calcite and dolomite. Davidite is isostructural with the crichtonite-group minerals, its association with rutile and both as principal opaque minerals. Davidite is present as up to 2 mm large zoned grains (Figure 12f). About 20 microprobe analyses have been carried out of davidite (Supplementary Materials Table S6). Its chemical composition is governed by Ti, V, Cr, and Fe-oxide accompanied by smaller amounts of REE, U and Pb. The major chemical components are TiO_2 (41.55–47.36 wt %) and FeO (15.38–19.66 wt %), and the U content ranges from 2.56 to 9.41 wt % UO_2 . The Th content is much lower, ranging from <0.01 to 0.19 wt % ThO_2 . Maximum amounts of other elements that were consistently detected include 0.92 wt % Sc_2O_3 , 3.31 wt % V_2O_5 , 12.06 wt % Cr_2O_3 , 0.68 wt % Y_2O_3 , 3.42 wt % La_2O_3 , 3.13 wt % Ce_2O_3 , 0.42 wt % CaO, 0.26 wt % MgO, 1.06 wt % SrO and 2.70 wt % PbO. Backscattered electron images of davidite display the presence of patchy compositional zoning and intense cracking of grains (Figure 13). It is not known whether the cracking is related to radiation damage induced volume expansion or to fracturing by tectonic processes. Reconnaissance EPMA traverses show that the compositional zoning, at least in part, reflects the distribution of Ti, Y, REE, U and Pb. Uranium, Cr, Ti and Pb tend to be relatively concentrated toward the central (more altered) portion of grains at the expense of Pb. Lighter areas thus have maximum U, Pb and minimum Ti, Y and REEs (Figure 13). REE appear to co-exist or substitute, respectively, for Pb and U, as indicated by the corresponding decreasing trends of Ti, Y, REE with increasing trend of Pb + U.

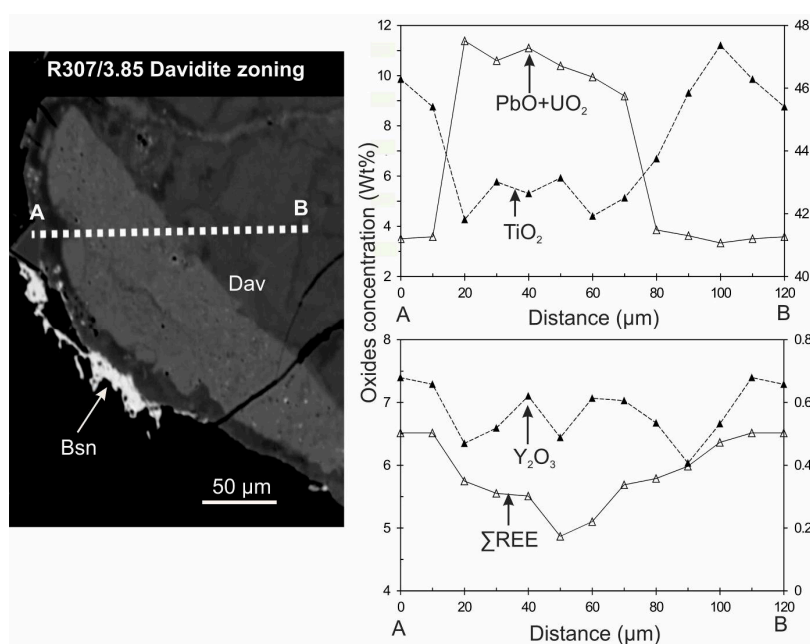


Figure 13. Back-scattered electron image of patchy chemical zoning of davidite (sample R307/3.85) as crichtonite group mineral. EPMA line scans across davidite zones corresponds to variation in the TiO_2 , $\text{PbO} + \text{UO}_2$, Y_2O_3 and REE contents.

3.4. REE Occurrences in Pegmatite and Greisen (Magmatic-Hydrothermal Systems)

3.4.1. Rapakivi Granite

Rapakivi granite occurs in four large batholiths (e.g., Vyborg, Aland, Vehmaa, Laitila) and several smaller satellite intrusions (e.g., Suomenniemi, Ahvenisto, Onas, Bodom, Obbnäs, Kökar, Fjälskär, Eurajoki, Kokemäki) in southern Finland [60]. In this study, we report comprehensive mineralogical and petrographic data from the Kymi Granite Complex within the Proterozoic Vyborg Rapakivi Batholith in south eastern Finland (Figure 14).

The rapakivi granite in the Kymi Complex hosts several greisen zones which are characterized by silicification with fine grained masses of sericite, muscovite and chlorite. Fluorite, topaz, zircon, epidote, apatite, genthelvite, iron-titanium oxides and sulphide minerals (sphalerite, galena, and chalcopyrite) are the most abundant accessory minerals. Geochemically, high F, Li, Rb, Ga, Sn and Nb, concentrations and depleted Mg, Ti, Zr, Ba, Sr and Eu contents distinct zones of greisen from the fresh granite [61]. Some of the greisens in rapakivi granite are also enriched in indium and rare earth elements, with roquesite (CuInS_2) being the major indium bearing mineral (Figure 15a), whereas monazite, allanite, bastnäsite, xenotime and thorite are the main REE rich minerals (Figure 15b–f).

The total REE content of greisens range from 100 to 1025 ppm with an average of 500 ppm [62], whereas the indium content is commonly from 70 to 200 ppm, but it may reach values of up to 800 ppm [54]. Previous studies concluded that enrichments of REE is due to a combination of magmatic and hydrothermal processes [60,63–65].

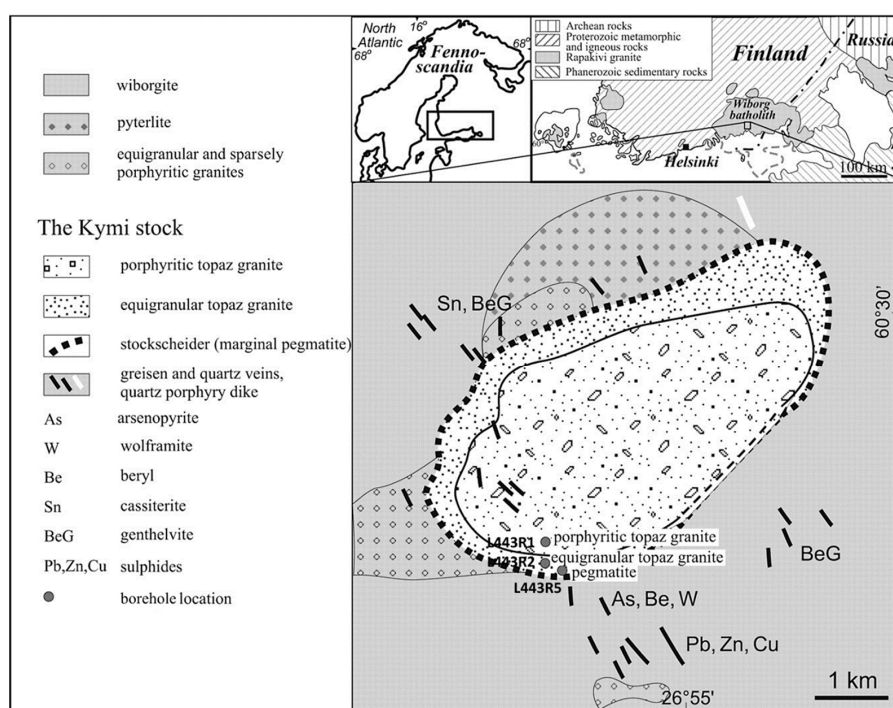


Figure 14. Geological map of the Kymi topaz granite stock in the Vyborg rapakivi batholith, south-eastern Finland. Modified from Lukkari et al. [64].

The 1.64–1.63 Ga Kymi Granite Complex can be divided into three varieties of rapakivi granite: (1) granite with ovoid alkali feldspar phenocrysts larger than 3 cm in diameter, mantled by sodic plagioclase. In this variety, the feldspar crystals have been partially re-melted, and subsequently altered; the alteration produced the rim of greenish sodic plagioclase; (2) granite with quartz-feldspar porphyritic texture and angular phenocrysts of potassium feldspar (microcline), plagioclase and quartz; (3) hornblende bearing granite with porphyritic rapakivi texture.

Detailed mineralogical observations on REE-bearing minerals were completed in 12 samples from the greisenised Kymi granite stocks and the surrounding country rocks (Figure 14). Results of electron microprobe analyses in those minerals are reported in the Supplementary Materials Table S7. Monazite occurs as euhedral to subhedral accessory crystals (20–50 μm diameter) and it is often intergrown with zircon, xenotime, apatite and fluorite (Figure 15b) and also fills fractures in apatite (Figure 15c). Monazite grains usually coexist with xenotime (Figure 15b). Contents of the major elements in monazite are as follows: P_2O_5 from 27.7 to 29.3 wt %, F from 1.0 to 1.6 wt %, Ce_2O_3 from 31.4 to 34.4 wt %, La_2O_3 from 11.7 to 15.4 wt %, Nd_2O_3 from 11.3 to 13.5 wt %, Sm_2O_3 from 1.3 to 2.7 wt %, Gd_2O_3 from 1 to 2.2 wt % and Pr_2O_3 from 3.0 to 3.6 wt %. The ThO_2 contents vary from 0.53 to 3.1 wt % whereas UO_2 has low concentrations from 0.01 to 0.24 wt % and SiO_2 varies between 0.5 and 3.2 wt % (Supplementary Materials Table S7).

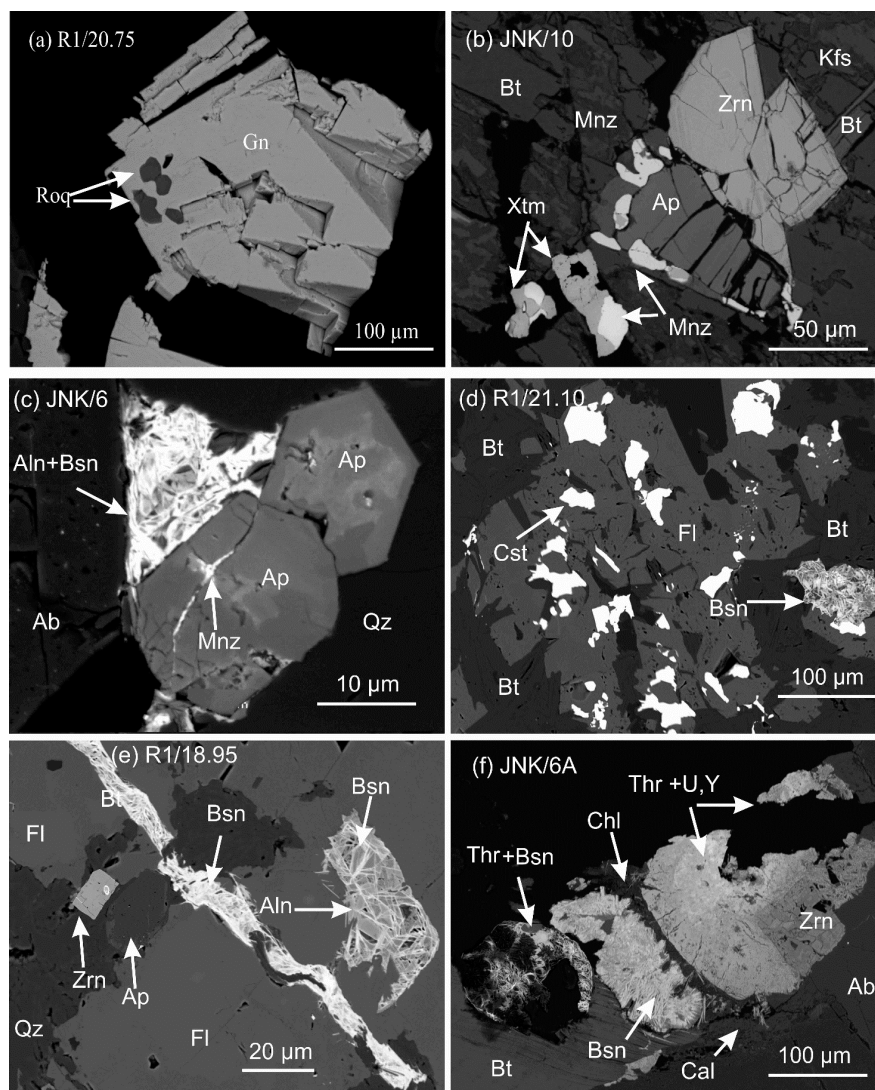


Figure 15. Back-scattered electron images REE-bearing minerals in Kymi granite stocks; (a) Cubic galena (Gn) crystals contain roquesite (Rq); (b) Coarse zircon (Zrn) crystals associated with apatite (Ap), monazite (Mnz) and xenotime (Xtm); (c) Hexagonal prismatic apatite (Ap), allanite (Aln) and bastnäsite (Bsn) intergrown in the outer rim of the apatite; (d) Bright inclusions of cassiterite (Cst) within fluorite (Fl); (e) Acicular/needle-like bastnäsite (Bsn) filling fractures within fluorite (Fl) and quartz (Qz); (f) Altered zircon associated with Y-Th-U minerals and bastnäsite (Bsn).

Bastnäsite is mostly present as disseminations of acicular and needle-shaped crystals and flakes ($100\ \mu\text{m} \times 300\ \mu\text{m}$). It also occurs in thin fractures and vugs of fluorite, biotite and quartz as round-hexagonal crystals (Figure 15c–e). Bastnäsite is commonly associated with allanite and thorite. At some places, bastnäsite appears to replace allanite as it forms rims around corroded allanite cores (Figure 15f). Bastnäsite is rich in LREE (~65 wt %), with Ce_2O_3 from 30.6 to 33.7 wt %, La_2O_3 from 12.9 to 17.9 wt %, Nd_2O_3 from 7.3 to 11.6 wt %, Sm_2O_3 from 0.8 to 2.0 wt %, Gd_2O_3 from 0.7 to 1.7 wt % and Pr_2O_3 from 2.5 to 3.2 wt % (Supplementary Materials Table S7). The fluor contents are between 6.7 and 9.3 wt %. Bastnäsite grains also contain significant amounts of total HREE (from 0.5 to 1.5 wt %), as well as ThO_2 (from 0.3 to 1.3 wt %) and Y_2O_3 (from 1.7 to 3.4 wt %).

3.4.2. Kovala Granitoid Complex

The Kovala Granitoid Complex is located in the Uusimaa Belt (1.85–1.79 Ga) in southern Finland (Figure 1). The complex has a well-developed zonal structure: the central part consists of coarse-grained equigranular to K-feldspar porphyritic biotite monzogranite and small granodiorite bodies, whereas the marginal zones of the complex consists of pyroxene gneiss. Garnet-cordierite gneiss as well as marginal pegmatite occur along the outer contact of the complex (Figure 16).

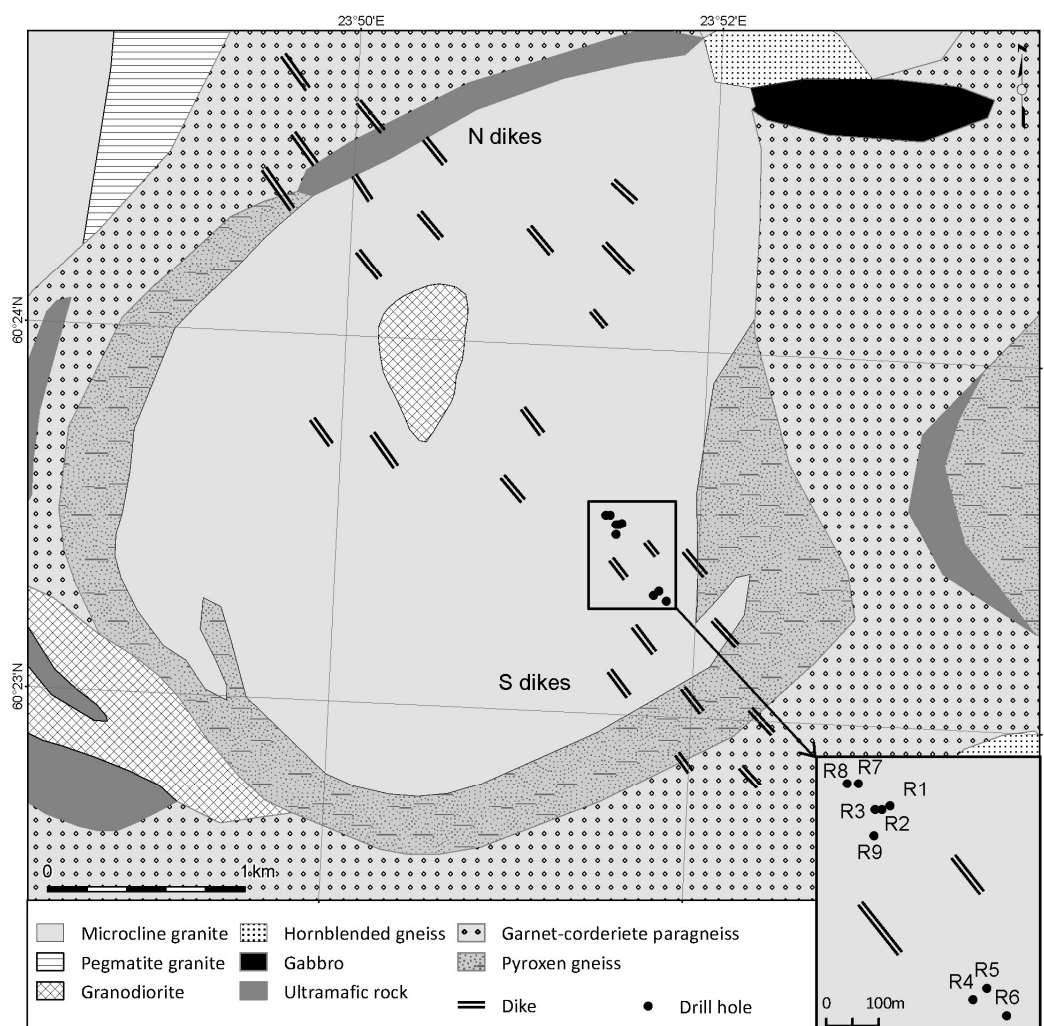


Figure 16. Geological sketch map showing the major lithological units of the Kovala granitic complex in southern Finland (also see Figure 1) on the basis of the electronic map sheet in the DigiKP database of the Geological Survey of Finland. Coordinates are given according to the Finnish National Coordinate System ETRS-TM35FIN.

The strongly radioactive granitic pegmatite bodies in the central part of the complex have predominantly peraluminous and S-type character. Most of the granitic pegmatite dikes run roughly in NW-SE direction and they are named according to their locations: S dikes in the southern part and N dikes in the northern part of the complex. These dikes are usually 5–10 m wide and 60–70 m long and gently dip to the West. Among them, the S dikes are more radioactive than the N dikes. They consist of perthitic K-feldspar, quartz, plagioclase, biotite, garnet, sillimanite, cordierite and staurolite. Monazite, zircon, xenotime, magnetite (oxidized), titanite, ilmenite and chlorite are the most common accessories. The complex underwent granulite facies metamorphism at 700–820 °C temperatures and 2.6–5.8 kbar pressures [66].

Monazite and Th-rich monazite are the most abundant accessories in the pegmatite dikes in addition to the commonly observed zircon, xenotime and huttonite/thorite. Monazite grains (100–1000 µm) are usually elongated or sometimes rounded and fractured. Their colours range from light yellow to yellowish brown. Exceptionally, some euhedral to subhedral prismatic crystals are as long as 3 mm (Figure 17a). Monazite is mostly enclosed in quartz and K-feldspar and attached to garnet (Figure 17b). Backscattered SEM imaging revealed complex sector-, concentric- and patchy-zoning, as well as normal growth zoning in monazite and presence of abundant thorite inclusions in some grains (Figure 17e–f). Growth zoning only rarely occurs, whereas concentric and patchy zoning have been recognized on monazites from most of the studied samples. Representative microprobe analyses of monazite compositions from the Kovela monzogranite and granite samples are given in Supplementary Materials Table S8. The zoning reflects the variations between the abundances of LREE and Th (+U + Ca and Si). Dark zones on SEM images of monazite predominantly occur as outer rims and as rare inner cores (Figure 17e). These zones have lower Th (+Ca and Si) and higher REE contents compared to the brighter zones. This negative correlation between Th (+Ca and Si) and REE occurs on all monazite grains and reflects the typical coupled substitution mechanisms in monazite: $(\text{Th}, \text{U})^{4+} + \text{Si}^{4+} \rightleftharpoons \text{REE}^{3+} + \text{P}^{5+}$ e.g., [67] and $(\text{Th}, \text{U})^{4+} + \text{Ca}^{2+} \rightleftharpoons 2\text{REE}^{3+}$ [68]. The A-site cation sites in the crystal structure of monazite are principally occupied by Ce as the dominant REE (from 24.90 to 28.56 wt % Ce_2O_3). The La-content varies from 8.30 to 10.56 wt % La_2O_3 and the Nd_2O_3 contents are from 8.98 to 10.54 wt %. The amount of Th, representing the huttonite molecule as a solid solution in monazite varies from 14.9 to 20.1 wt % ThO_2 . The U content is low and ranges from 0.47 to 1.47 wt % UO_2 . The Ca content, representing the cheralite molecule as a solid solution in monazite, varies from 0.71 to 1.69 wt % CaO. Skeletal and porous intergrowths of 10–20 µm large crystals of thorium-silicate compositions (probably huttonite or thorite) with monazite were also observed by SEM (Figure 17f). The huttonite grains contain from 52.7 to 66.0 wt % ThO_2 as main component, with several weight percent of LREE (1.3–7.4 wt % Ce_2O_3 , 0–1.6 wt % La_2O_3 and 0.7–2.1 wt % Nd_2O_3 ; Supplementary Materials Table S8). The P and U contents in huttonite grains vary from 3.2 to 6.5 wt % P_2O_5 and from 0.9 to 2.9 wt % UO_2 , respectively. The percentage of monazite, cheralite and huttonite components in these thorium-silicate grains range between 5.0–18.2 wt %, 13.0–27.0 wt %, and 62.1–74.4 wt %, respectively.

Thorite forms inclusions within monazite and zircon (Figure 17a,b). Two types of zircons were found: (1) small (<50 µm) grains with round to subhedral habits as inclusions in garnet and monazite (Figure 17a–c); and (2) coarse, from 100 to 400 µm large crystals with mostly euhedral to subhedral prismatic shapes. Type 2 zircons often show oscillatory zoning on BSE images (Figure 17c). The elevated Th contents in the Kovela complex was most probably resulted from a complex, multi-stage process which involved primary magmatic crystallization and superimposed metamorphic-hydrothermal alteration. Förster and Harlov [69], Overstreet [70], Mohr [71] and Kelly et al. [72] suggested that metamorphism may generate the breakdown of primary monazite to Th-rich mineral in the monazite-huttonite series by depletion of the Y, HREE, Ca and P content parallel with the relatively enrichment of Th, Si and LREE.

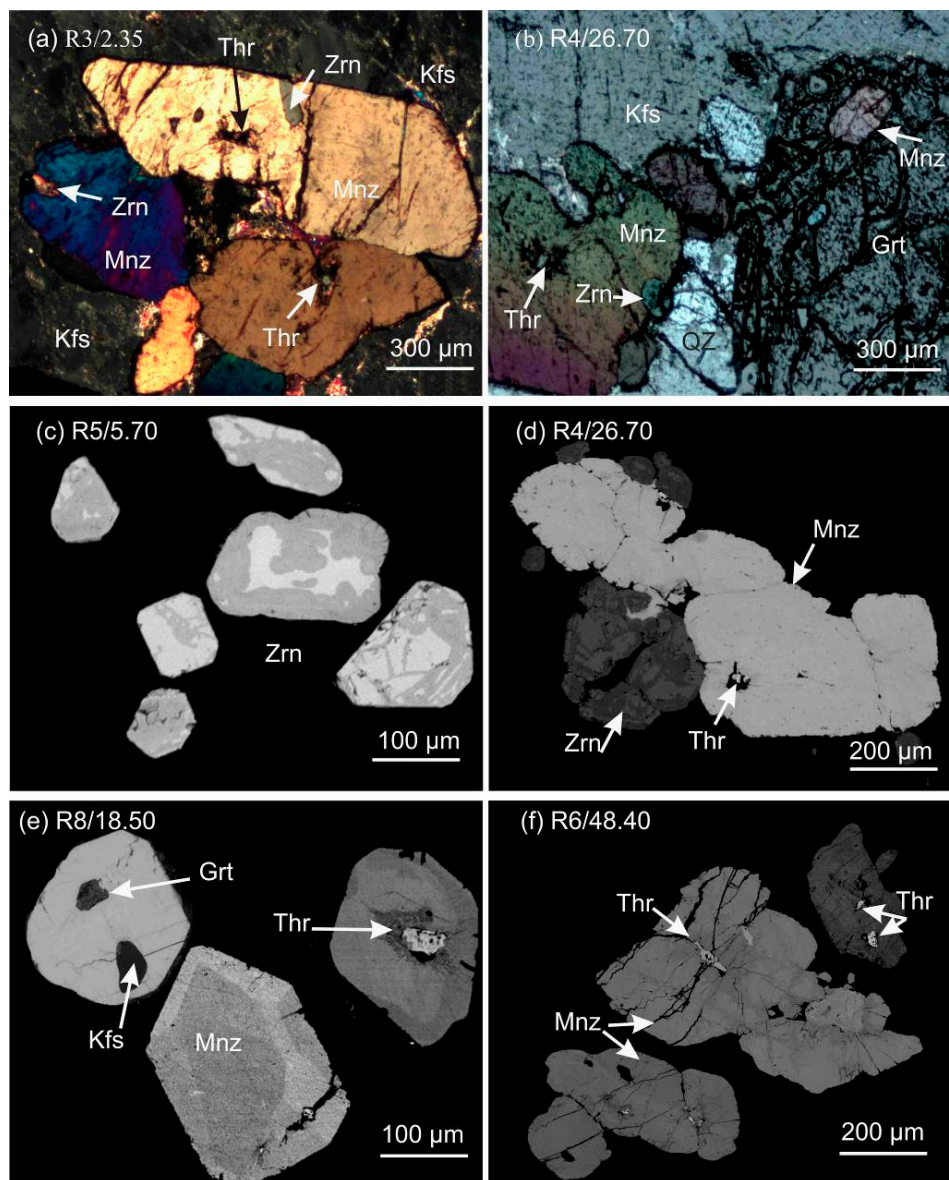


Figure 17. Polarizing microscope and back-scattered electron images of REE-bearing minerals in the monazite bearing granite at Kovala; (a,b) Coarse hexagonal and elongated monazite (Mnz) overgrowth with other monazite in contact with feldspar (kfs), quartz (Qz) and Garnet (Grt); (c) Euhedral to subhedral zircon (Zrn), shows typical oscillatory zoning and/or sector zoning; (d) Monazite (Mnz) intergrown with zircon (Zrn); (e) Monazite crystals illustrating zoning types and different inclusions; (f) Thorium-silicate materials occurring as inclusions or as disseminated crystals within monazite grains.

4. Compositions of REE Minerals with Different Origins in Finland

Box-plot diagrams of REE concentration data according to the main REE-bearing phases from the studied deposits and occurrences in Finland are shown in (Figure 18). As it is expected, and also demonstrated by many other studies [63,64], LREE are generally enriched in monazite, allanite and carbonate minerals, whereas xenotime concentrates HREE regardless the conditions of crystallization. The highest average LREE concentrations at around 60 wt % occur in monazite, bastnäsite and synchysite, but the range of these values is highly variable. However, comparison of mantle-normalized [73] REE distributions in different types of REE-rich minerals from carbonatite and alkaline rocks, hydrothermal

alteration zones and granitoids/greisen with elevated REE contents reveals significant and systematic variation in both absolute and relative abundances (Figure 19). The REE distribution patterns of bastnäsite, allanite and ancylite are similar to those of monazite. They are characterized by higher LREE over HREE, and negative Y anomalies. In each types of minerals, except of xenotime, strong enrichment in LREE relative to MREE and HREE can be clearly seen. The normalized plots for most monazite exhibit similar patterns in each types of deposits/occurrences, but monazite from granitoids-related magmatic-hydrothermal (e.g., pegmatite and greisen) systems have higher REE contents in comparison to the metasomatic-hydrothermal and carbonatite related environments (Figure 19a). Allanite and ancylite show similar REE patterns to monazite, with the lowest concentrations of REE in alkaline-rocks and carbonatite in comparison to the other types of geological environments (Figure 19b). Similarly to monazite and allanite, bastnäsite and synchysite also display steeply right-inclined normalized REE profiles with depleted Y contents (Figure 19c,e), but bastnäsite from pegmatite/greisen shows lower REE concentrations in comparison to the other geological environments.

HREE concentrations above the detection limits of the EPMA analyses characterize the pegmatite/greisen hosted monazite, allanite and bastnäsite only. However, the absolute HRRE concentrations are just around or even lower than those in the average of the mantle [72]. Strong enrichment of HREE over LREE characterize xenotime (Figure 19f). This reflects that xenotime prefers to incorporate HREEs into its structure [74].

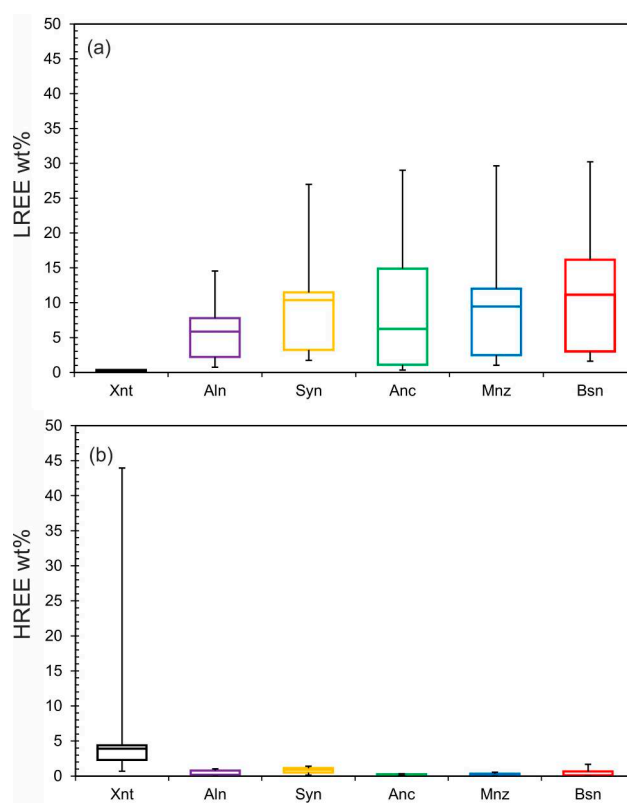


Figure 18. Box plots showing the distributions of REE concentrations in REE-bearing phases of the studied rocks (a) Distribution of total LREE; (b) Distribution of total HREE.

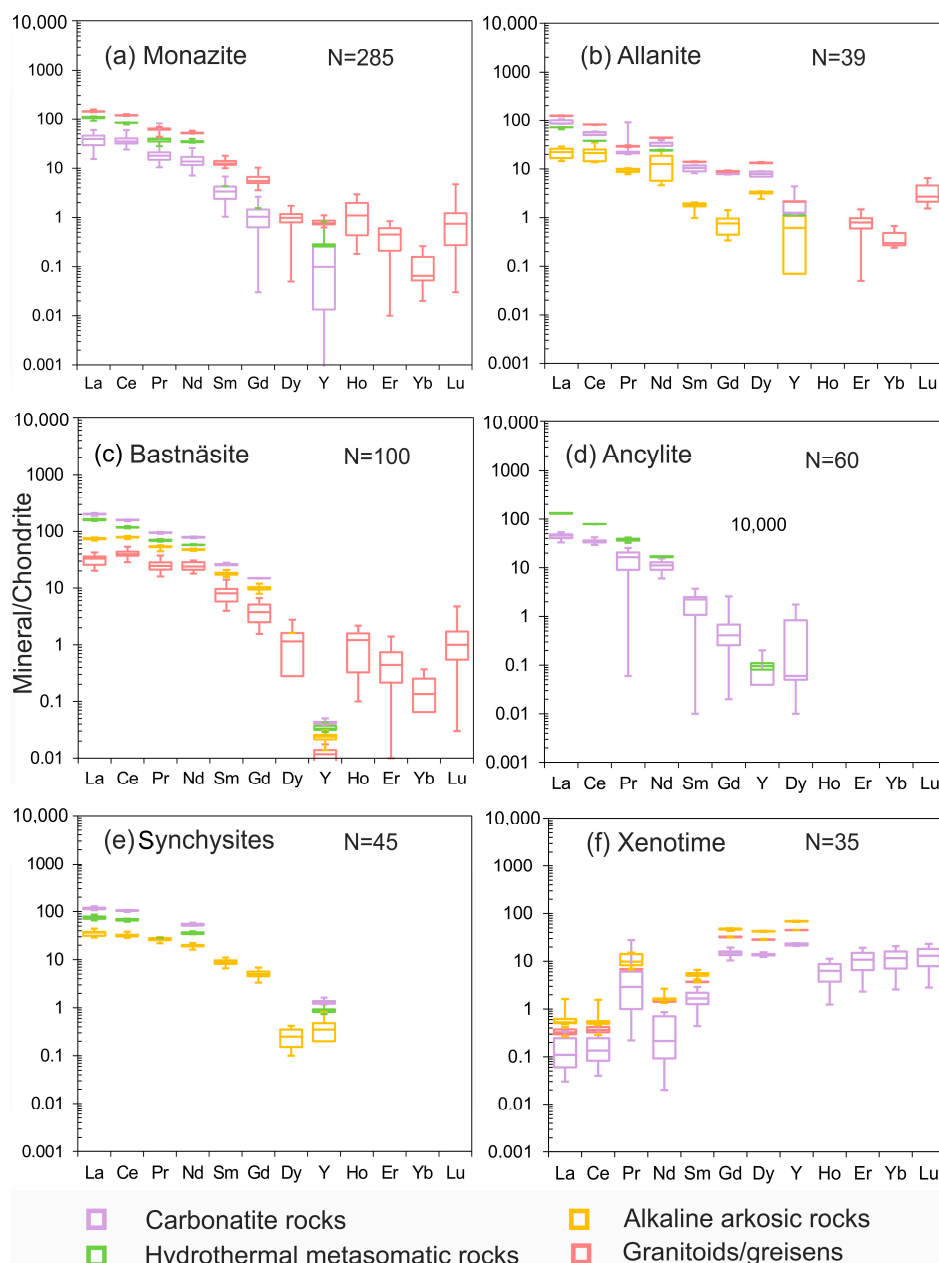


Figure 19. Normalized REE distribution diagrams for average chondrite-normalized REE patterns of (a) monazite, (b) allanite, (c) ancyllite, (d) bastnäsite, (e) synchysite and (f) xenotime. Chondrite values normalized relative to mantle compositions after McDonough and Sun [73].

The differences in REE-enrichments and CaO-contents according to the origin of the REE rich phosphate minerals are also evident in the LREE–HREE + Y–CaO ternary plots (Figure 20). Monazite from the carbonatite has a relatively wide range in the proportions of the different HREE+Y and LREE, as well as total REE and CaO contents (Figure 20a). This variability in composition probably reflects the cumulative effect of fractionation of REE during crystallization of carbonatite melts with different composition, as well as the effect of segregation of magmatic fluids. Under magmatic conditions, dolomite has lower partition coefficients for REE than calcite [3], and precipitation of rock forming carbonate minerals results in enrichment of LREE in the residual liquid. La-Ce and Sm-Nd also fractionate into magmatic fluids in different proportions [75]. In contrast, monazite

from hydrothermal and granite-related magmatic-hydrothermal environments appear to show less variability in composition with dominance of LREE (Figure 20a).

Xenotime in carbonatites, alkaline rocks and granite related magmatic-hydrothermal systems also exhibits limited, although specific variations in the relative concentration of HREE + Y to LREE (Figure 20b). The source of elements for the formation of xenotime-(Y) in the studied granitic rocks is the leaching of P, REE and Y mainly from zircon and apatite. Monazite and apatite associated with xenotime related to the breakdown of primary (Fe, U, Y, REE, Ca, Si)-(Nb, Ta) oxide phases both tend to have slightly higher LREE compared to most xenotime grains. The latter type is also clearly higher in the HREE and lower in Y.

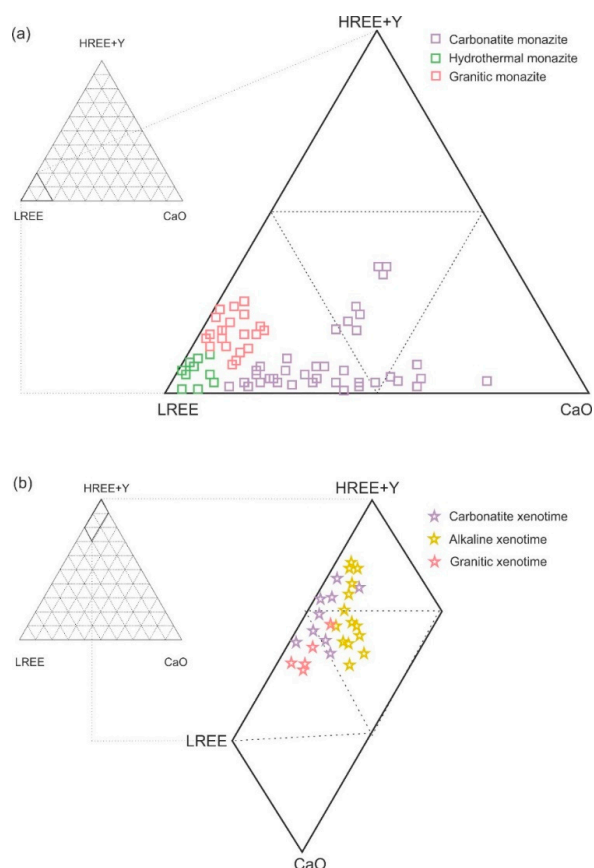


Figure 20. Compositions of monazite (a) and xenotime (b) in (LREE)–(HREE + Y)–Ca ternary diagrams (mol %); from different types of REE deposits and occurrences in Finland.

In the REE deposits of occurrences of Finland, bastnäsite and synchysite are the most common Ca-REE fluorocarbonates and they also show compositional variation according to the conditions of their crystallization (Figure 21a). Based on the EPMA data, bastnäsite with low Ca + Sr contents, ranging from 0.1 to 1.1 wt % CaO + SrO (hydrothermal), 2.0 to 7.3 wt % CaO + SrO (carbonatite), 0.1 to 6.2 wt % CaO + SrO (granitic), 3.6 to 6.1 wt % CaO + SrO (alkaline) and synchysite, with higher Ca, varying between 11.7 and 18.0 wt % CaO + SrO (hydrothermal) 11.8 and 17.6 wt % CaO + SrO (carbonatite), 8.6 and 13.5 wt % CaO + SrO (alkaline) respectively. Both minerals are classified as fluorocarbonates with F dominant in the F–OH–Cl site. Compositions of the Ca-REE fluorocarbonates (bastnäsite and synchysite) also discriminate formation conditions in the LREE–HREE–CaO ternary diagram, but in a different and less straightforward way (Figure 21a). Hydrothermal and carbonatite bastnäsite are richer in LREE in comparison to synchysite of similar origin, whereas the compositional differences considering the LREE and CaO contents are less pronounced in the pegmatite/greisen and alkaline rocks hosted occurrences. The less pronounced differences among REE-carbonates from

different geological environments most probably reflect the complex effect of temperature-pressure and CO_2 concentration parameters [48]. On the basis of our investigations at the REE occurrences and prospects in Finland, we suggest that high mole fractions of CO_2 in a hydrothermal fluid also enhanced such fractionations, again due to the greater solubility of neutral complexes in fluids of low dielectric constants.

Figure 21b shows the compositions of REE silicate minerals (allanite-ferroallanite, and chevkinite) of different origin in the (Y + REE)–(Al + Fe)–(Ti) ternary. Most of the allanites in studied REE occurrences and prospects belongs to the allanite-ferriallanite series (up to 40% of allanite-Ce), and a smaller part, to the ferriallanite end-member (Figure 21b). The CaO content of allanite-(Ce) is unusually high and appears to be a characteristic feature of allanite from arkose gneiss in Tana Belt.

Chevkinite, which has the same crystal system as allanite contains more titanium than allanite and ferroallanite, and this Ti-enrichment of allanite-type silicates characterize chevkinite grains in carbonatites and albitite alteration zones in hydrothermal systems. The distribution of allanite and chevkinite in the studied carbonatites dikes suggests that the composition of the magmas is an important control on the stability fields of these minerals, a fact that is supported by the presence of primary allanite in rocks formed by processes of mixing magmatic fluids and a later hydrothermal fluid. Bagiński et al. [76] and Macdonald et al. [77] documented the alteration of chevkinite-(Ce) to a phase strongly enriched in Ti and depleted in Si, REE and Fe compared to the unaltered phase. In contrast to studies chevkinite did not alter to a member of the epidote-group, possibly because REE + Y abundance in chevkinite (43–50 wt %) is almost twice that observed in allanite.

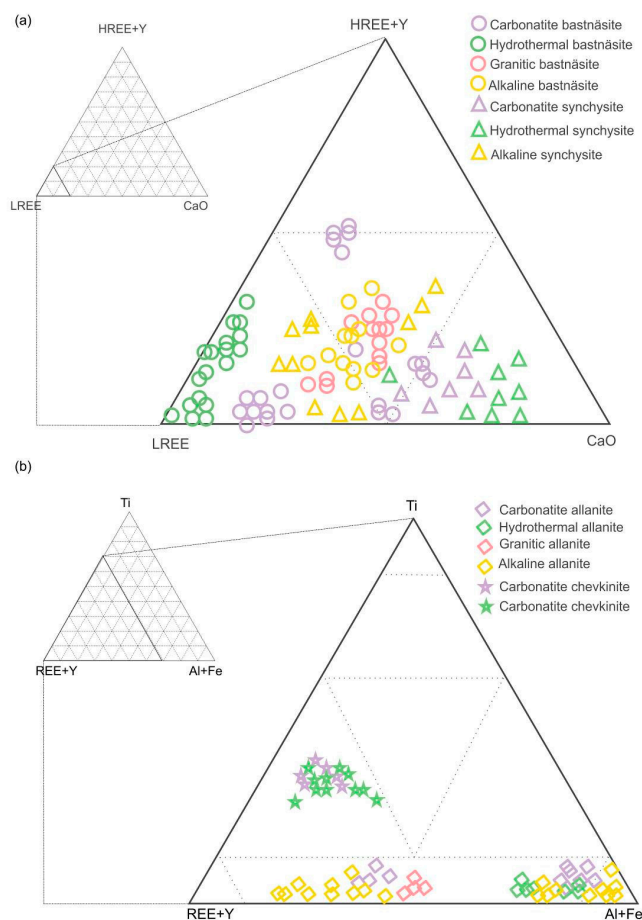


Figure 21. Compositions of Ca-REE fluorocarbonates in the (LREE)–(HREE + Y)–Ca ternary diagram (mol %) (a); and REE silicate minerals in the (REE + Y)–Ti–(Al + Fe) ternary diagram (mol %) (b); from different types of REE deposits and occurrences in Finland.

5. Comparison of Results from Finland with Published Compositional Data of Carbonates, REE-Phosphates and Silicates from Other Areas

The $(La/Nd)_{cn}$ ratio in REE-fluorocarbonates is used to identify and define variable hydrothermal systems, as an indicator of the paragenetic type of occurrence and geological environment and REE fractionation within, or between deposits [3,78–82]. The mean values of $(La + Ce + Pr)/(\Sigma REE)$ and $(La/Nd)_{cn}$ obtained from the present datasets (a total of several thousand analyses presented in the Supplementary Materials Tables), are summarized in Table 2, and are compared with measured ratios from published compositional data. However, the wide ranges in the $(La/Nd)_{cn}$ of REE minerals from the studied areas, indicate substantial fractionation of these elements in the most important metallogenic provinces and prospecting target of REE deposits in Finland. The wide variations also occur for specific minerals, even within a single sample or grain, indicating changing compositions of the fluid during crystallization.

Smith et al. [3] have discussed fractionation of La and Nd during hydrothermal mineral-forming processes, using data from the Bayan Obo REE deposit in China. According to their model, variations in the relative proportions of these elements are primarily related to REE speciation in the fluids and temperature conditions. At high temperatures ($>250\text{ }^{\circ}\text{C}$) and in a CO_2 -rich fluid, La-bearing fluoride complexes have a higher association-constant than, for example, for Nd, promoting the observed fractionation.

Table 2. The ratios of $(La/Nd)_{cn}$ and $(La + Ce + Pr)/(\Sigma REE)$ in REE minerals from the studied areas compared to measured ratios from other world's REE deposits.

| Mineral | $(La + Ce + Pr)/(\Sigma REE)$ | $(La/Nd)_{cn}$ | Mineral | $(La + Ce + Pr)/(\Sigma REE)$ | $(La/Nd)_{cn}$ |
|---------------------------------------|-------------------------------|----------------|---------------------------------------|-------------------------------|----------------|
| Monazite | | | Allanite | | |
| Carbonatite rocks | 0.80 | 0.80–4.55 | Carbonatite rocks | 0.75 | 2.17–2.98 |
| Hydrothermal metasomatic rocks | 0.85 | 2.05–4.17 | Hydrothermal metasomatic rocks | 0.87 | 6.87–9.26 |
| Granitoids/greisens | 0.75 | 1.57–2.27 | Granitoids/greisens | 0.77 | 2.09–2.71 |
| Alkaline rocks | 0.77 | 2.03–2.26 | Alkaline arkosic rocks | 0.71 | 1.05–4.23 |
| Nechalacho | | | Alkaline rocks, Nechalacho | 0.83 | 2.8–2.9 |
| Hydrothermal ore, Olserum-Djupedal | 0.70 | 0.60–2.50 | Carbonatite, Bayan Obo | 0.86 | 3.8 |
| Carbonatite, Bayan Obo | 0.85 | 4.50–6.20 | Pegmatite Creek Pass | 0.72 | 1.70–3.40 |
| Pegmatite, Creek Pass | 0.63 | 1.48–1.51 | Hydrothermal ore, Olserum-Djupedal | 0.74 | 1.67–2.48 |
| | | | Upper Crust | 0.68 | 1.2 |
| Bastnäsïte | | | Synchysite | | |
| Carbonatite rocks | 0.78 | 0.50–3.66 | Carbonatite rocks | 0.78 | 1.49–3.43 |
| Hydrothermal metasomatic rocks | 0.89 | 8.50–12.84 | Hydrothermal metasomatic rocks | 0.80 | 1.94–3.43 |
| Granitoids/greisens | 0.70 | 0.80–2.00 | Alkaline arkosic rocks | 0.71 | 1.56–2.37 |
| Alkaline arkosic rocks | 0.73 | 1.71–2.21 | Alkaline rocks, Nechalacho | 0.76 | 1.73–2.26 |
| Alkaline rocks | 0.79 | 2.22–2.28 | Carbonatite, Bayan Obo | 0.79 | 0.60–2.20 |
| Nechalacho | | | Hydrothermal ore, Olserum-Djupedal | 0.84 | 2.0–2.3 |
| Hydrothermal ore, Olserum-Djupedal | 0.72 | 1.70–2.38 | Upper Crust | 0.68 | 1.2 |
| Upper Crust | 0.68 | 1.2 | | | |

Result of our studies in Finland indicate origin-dependent distribution of REE minerals composition on the plots presenting $(La/Nd)_{cn}$ ratios against the $(La + Ce + Pr)/(\Sigma REE)$ ratios (Figure 22; Table 2). These results compare favorably with published data from the carbonatite dikes at Bayan Obo in China [3], alkaline/peralkaline igneous rocks hosted REE deposit at Nechalacho in NW Canada [78], the Olserum Djupedal REE-phosphate mineralization of hydrothermal origin in SE Sweden [79], and granite related pegmatite hosted deposit at Creek Pass, Colorado [80]. The highest ratios occur in REE minerals of hydrothermal origin and similarly high ratios was found in monazite and synchysite from carbonatites only. Monazite from the Finnish carbonatite deposits is characterized

by a wide range of the proportions of lanthanides ($La + Ce + Pr / \Sigma REE$ At %) and $(La/Nd)_{cn}$ ratios compared to other monazite samples from different occurrences (Figure 22a). This probably reflects fractionation of REE between melts, fluids and monazite during the crystallization of the parent carbonatite melts, similarly to the fractionation trend observed by Smith et al. [3] at Bayan Obo. Monazite from granite-related environments (e.g., pegmatite and greisen zones) in Finland is characterized by a relatively narrow $(La/Nd)_{cn}$ and $(La + Ce + Pr) / (\Sigma REE)$ ratios (from about 2 to 1.5 and less than 0.75, respectively), close to the values of the average upper crust (e.g., 1 and 0.68, respectively). These ratios are similar to those for monazite from REE deposits occurring in alkaline rocks, pegmatite and hydrothermal veins outside of Finland (Figure 22a).

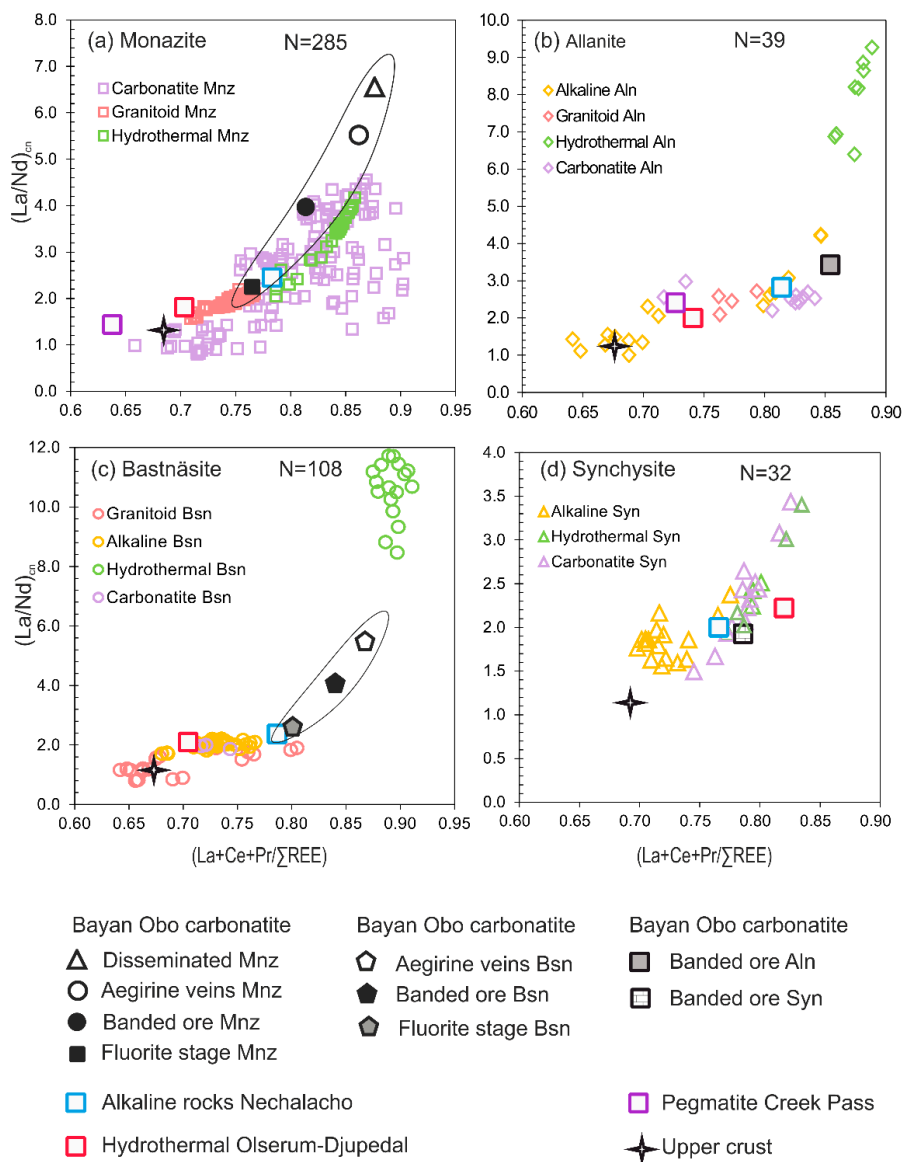


Figure 22. Composition plots showing $(La/Nd)_{cn}$ ratios against $(La + Ce + Pr / \Sigma REE)$ ratios in the studied REE minerals of different origin in Finland and the averages of these ratios from REE deposits outside of Finland. Sources of data for deposits outside of Finland are referred in the text. The average upper crust data are from [71]. (a) Monazite, the fractionation trend observed by [3] at Bayan Obo is highlighted by the black ellipse. (b) Allanite, (c) Bastnäsite, The fractionation trend observed by [3] at Bayan Obo is highlighted by the black ellipse. (d) Synchysite.

Allanite from hydrothermal occurrences in Finland is lanthanum-enriched, relative to other allanite of different origin (Figure 22b). Compositions of allanite from carbonatites, alkaline rocks and greisens are characterized by relatively low $(La/Nd)_{cn}$ ratios (between 3 and 1) and low $La + Ce + Pr/\Sigma REE$ ratios (less than 0.85) and fall into the compositional trend defined by the average data from the Nechalacho (alkaline rock hosted), Olserum Djupedal (hydrothermal) and Creek Pass (pegmatite) deposits.

Bastnäsite from different types of REE deposits and occurrences in Finland shows the widest ranges in $(La/Nd)_{cn}$ starting from about crustal values, as shown in granitoids/greisens rocks ($(La/Nd)_{cn} = 0.80$ to 2.0) and going to the maximum ratios encountered, as in hydrothermal metasomatic rocks ($(La/Nd)_{cn} = 8.5$ to 12.84). The rapidly changing conditions that would prevail in high temperature metamorphic hydrothermal fluids with highly variable CO_2 -content provide an explanation for the large compositional variations found on the bastnäsite compositions from different REE deposits. The REE distribution in bastnäsite-(Ce) from the carbonatite deposits, granitoids/greisens and alkaline arkosic rocks in Finland have similar patterns of variation compared to alkaline rocks at Nechalacho and hydrothermal deposits at Olserum-Djupeda, but plotting below the fractionation trend observed in the Bayan Obo carbonatite (Figure 22c; Table 2).

Synchysite from Finnish carbonatite, alkaline rock hosted and hydrothermal deposits have relatively wide ranges of La/Nd_{cn} ratios (from around 3.4 to 1.5) and $La + Ce + Pr/\Sigma REE$ ratios (between 0.85 and 0.6) and these ratios largely corresponds to those from different deposits from Finland (Figure 22d).

6. Discussion

Despite of the existence of several areas with high REE potential and many ongoing exploration projects, the territory of Finland is still underexplored for REE. However, if demand is to be met in the future, continued research into, and further exploration of Finnish REE resources will be needed. The REE exploration potential in Finland may be evaluated by comparing the geochemical databases and known REE occurrences with global deposit types. In terrains which are largely covered by glacial or other young unconsolidated sediments, such as the area of Finland, mostly geochemical and geophysical methods are used for localization of areas with REE potential. The most probable pathway to REE production in Finland is via the by-production alongside with extraction of other commodities such as P, Nb, Ta and Au. Enrichment of the REE may occur through primary processes such as magmatic processes and hydrothermal fluid mobilization and precipitation, or through secondary processes that move REE minerals from where they originally formed, such as sedimentary concentration and weathering.

Several REE deposits and occurrences in various geological settings across Finland have been subjected to detailed geological and mineralogical studies. These REE resources are intimately associated with a variety of rock types such as late-stage carbonatite dikes, epigenetic-hydrothermal systems and granite-pegmatites and greisens. The main features of the major REE-bearing minerals from the REE-bearing deposits obtained in this study have been summarized in Table 1. Primary magmatic REE enrichments occur in late-stage carbonatite dikes in the Sokli carbonatite complex (1–10 wt % RE_2O_3), with carbonatite veins at the Korsnäs deposit (0.9 wt % RE_2O_3), alkaline gneiss at the Otanmäki-Katajakangas deposit (2.4 wt % RE_2O_3) and monazite granite in Kovala (0.5–4.3 wt % RE_2O_3). Hydrothermal REE deposits are also of interest, although typically low-grade; they include Fe-oxide-Cu-Au class deposits in the Paleoproterozoic Kuusamo Belt (Au, Cu, Mo, Ni, REE and U), and Tana Belt in Northern Finland. These deposits could be potential sources of REE as a by-product of Au and other metals. Higher concentrations of the REE are found in the Kortejarvi and Laivajoki carbonatite intrusions, whereas A-type granite intrusions within Vyborg rapakivi batholith display high average levels of Sn, Ga, Nb, Be, In and REE [12,60]. According to the existing mineralogical and geochemical data, the Eurajoki and Kymi stocks seem to have the most potential for REE mineralisation among the rapakivi granites.

The late stage carbonatite dikes in the Sokli complex (360–380 Ma), located in the Finnish part of the Devonian Kola alkaline province, contain one of the most diverse assemblages of REE minerals described so far from carbonatites and provide an excellent opportunity to track the evolution of late-stage carbonatites and their sub-solidus (secondary) changes. More than ten different types of rare earth minerals have been analysed in detail and compared with analyses published from other deposits. Most of these minerals common in carbonatites (e.g., Ca-REE fluocarbonates and ancylite-(Ce)) plus monazite, xenotime and Sr, REE-apatite and some of them are very rare Ba, REE fluocarbonates. Mineralogical and mineral chemical evidence demonstrates that hydrothermal and metasomatic reworking processes were responsible for the REE mineralization in Sokli carbonatite veins and confirms that such processes are predominant in the formation of REE minerals in carbonatites. During late-stage processes, apatite and carbonate minerals were replaced by various assemblages of REE-Sr-Ba minerals. Other example is the Korsnäs Pb-REE-bearing carbonatite dyke which intrudes Palaeoproterozoic mica-gneisses of the Pohjanmaa schist belt, and hosts REE-bearing apatite, monazite, allanite, calcio-ancylite, and bastnäsite. The deposit consists of mineralised zones in pegmatite and carbonatite or calcareous scapolite-diopside-barite-bearing skarn rocks. The wall rock of the dyke has been kaolinised in the strongly sheared ore zone. Apatite and monazite are heterogeneously distributed in the ore but occur together with galena. Monazite forms either anhedral grains or larger grain clusters that occur as inclusions within apatite phenocrysts.

In contrast to carbonatites, other notable examples of REE-rich products of the peralkaline rocks include REE-P deposits in Otanmäki Katajakangas deposit south of the Lake Oulujärvi in central Finland. It is not surprising, that in addition to monazite and allanite, which are typical LREE hosts in the studied rocks, the peralkaline varieties contain such HREE minerals as fergusonite-Y and fergusonite-U. Other notable heavy rare-earth element (REE) hosts include primary zircon and columbite. Hydrothermal reworking and autometasomatic processes have been reported to produce HREE mineralization (e.g., fergusonite-Y, and euxenite-Y) arising from the decomposition of allanite and other primary Nb, Ti minerals [81,82]. On the other hand, rare-metal minerals are hosted by the granites of both the older and younger phases and produced by a combination of anatexis (principally silicate minerals, as allanite) and later hydrothermal processes (mostly oxide minerals, as fergusonite). Furthermore, fractionation of rare-earth elements in allanite-(Ce) and monazite-Ce led to magma enrichment in middle and heavy rare earths, leading to the crystallization of fergusonite-Y, and euxenite-Y during the late magmatic stages.

Hydrothermal alteration zones associated with Au-Co-Cu \pm U mineralization in the central part of the Kuusamo belt is characterized by REE and U-rich minerals. There are two stages in the evolution of Au-Co-Cu \pm U deposits within the Kuusamo Belt. The first conforms to a classic magmatic scheme, the second is postmagmatic and is characterized of multiphase metasomatism and metamorphic hydrothermal processes. In the postmagmatic stage, albitization, sericitization, chloritization, carbonation, and silicification have been traced [16,57]. Albitisation is the most extensive alteration type and is, apparently, preceded the establishment of peak metamorphic conditions of the Svecofennian orogeny. Several phases of mineralization appeared in conjunction with albitization, resulting the enrichments in niobium, yttrium, uranium, thorium and REE. Niobium mainly situated in pyrochlore, fergusonite, and titanite. The uranium content is high in some minerals (uraninite, with 78.6 to 80.5 wt % UO₂, davidite, euxenite, cloumbite), while thorium concentrated in other ones (thorite, monazite allanite). Albitization is followed by the chloritization, which is closely related to gold mineralization and indicated by the formation of chlorite, tremolite-actinolite, magnetite, talc and Fe sulphides. Chloritized rocks exhibit enrichments in heavy REE, and are relatively strongly enriched in Mg, strongly depleted in Si and large ion lithophile (such as U, Th, Nb, F) elements, and slightly depleted in light REE. The next stage is phyllic alteration, indicated by biotite and sericite \pm pyrite and additional gold mineralisation and ductile deformation. Sericitized rocks were previously silicified; they are very strongly enriched in K-Rb-Cs-Ba, very strongly depleted in Na-Ca-Sr-Eu, and slightly depleted in light REE relative to albitization stage. This is followed by a

stage of carbonation, silicification, where calcite, allanite-Ce, ancylite-Ce, and bastnäsite-Ce replace monazite-(Ce) after apatite. Alterations are localized on permeable zones such as fractures, flow tops, discordant breccia dikes, and conformable breccia horizons.

In addition to peralkaline granites (see above), their late-orogenic peraluminous counterparts in post- or anorogenic settings may be associated with Vyborg granites and granite pegmatite (Kovela) with high Th-LREE content. The Vyborg rapakivi batholith (1.64 Ga) in south-eastern Finland (Kymi) is one of a few regions in the Fennoscandian Shield with several documented occurrences of REE, indium and Zn-Cu-Pb sulphide mineralization. The late-orogenic peraluminous Kovela monazite-granite shows up as a strong positive aeroradiometric gamma radiation anomaly in the Svecofennian Uusimaa Belt. Monazite is the dominant REE-mineral; accessory minerals include zircon, xenotime, and thorite.

7. Conclusions

The most significant REE deposits and occurrences in Finland are associated with highly fractionated carbonatite intrusions and dikes, alkaline rocks, hydrothermal alteration zones in metamorphic rocks and greisens and pegmatites in granite intrusions. The most common REE minerals and REE-bearing minerals in these environments are phosphates (monazite, xenotime and fluorapatite), fluorocarbonates (bastnäsite and synchysite), hydrated carbonates (ancylite), hydrated aluminium silicates (allanite, Fe-allanite, cerite, chevkinite), oxides (fergusonite, euxenite) and U-Pb rich minerals.

Late-stage carbonatite dikes in the Sokli carbonatites are important sources of REE in Finland. Less pronounced that LREE enrichment is found in the metasomatic carbonatite bodies at Sokli and calcsilicate rocks (skarn) from Korsnäs. On the basis of variations in REE distributions and mineral chemistry, strong differentiation of REE contents in monazite can be distinguished in the carbonatite complexes in Finland and elsewhere. Other REE rich minerals from the magmatic and post-magmatic stages of carbonatite complexes show less pronounced variations in REE contents.

Alkaline rocks (Otanmäki) have potential for occurrences of significant REE deposits. The host alkaline granitic rocks are typically formed by progressive fractional crystallization of a parental magma and the deposits typically represent two periods of mineralization. The first primary magmatic period is associated with crystallization of highly fractionated magma rich in REE. The minerals of this period are commonly overprinted during the second period by late magmatic to hydrothermal fluids enriched the primary mineralization and remobilized REE in to hydrothermal veins.

The epigenetic hydrothermal alteration and associated REE enrichments are documented in the Kuusamo Belt. Several phases of REE mineralization can be distinguished. Subtle compositional differences among REE-fluorocarbonates (bastnäsite, synchysite), monazite and allanite define a spectrum from relatively La-enriched to (Ce + Nd)-enriched phases. The La-rich character of the mineralization in the Kuusamo Belt may be related to the high CO₂-contents of high temperature metamorphic–hydrothermal fluids as high coordination number complexes of La are predicted to be more strongly associated than for the other REE [3].

The pegmatite dikes within Kovela granitic complex, southern Finland are characterized by the presence of Th enriched monazite and its specific compositional variation (huttonite/thorite monazite) appears to represent multi-stage process which involved primary magmatic crystallization and late-stage hydrothermal alteration. The recrystallization during both the high-T and lower-T magmatic-hydrothermal events, led to monazite becoming depleted in Y, HREE, Ca and P, and relatively enriched in Th, Si and LREE to form the Th-rich minerals of the monazite huttonite series.

In the greisens of rapakivi granite in the Kymi stock, LREE are carried by monazite, bastnäsite and allanite, and the HREE by xenotime and zircon. The REE-mineralization was also formed by the combination of magmatic and post magmatic processes.

The fractionation processes leading to high variation in lanthanum contents of monazite in carbonatite hosted REE-rich deposits (e.g., Bayan Obo) was also observed in Finnish deposits. Results of studies in Finnish deposits and occurrences suggest that origin of REE-bearing minerals can be

distinguished on the basis of the chondrite-normalized REE patterns, as well as on the basis of relative variation of LREE and HREE concentrations in relation to some major elements (Al, Ti, Fe, Ca). The exceptional high enrichment of LREE, HREE, U, Th and Y in various minerals is restricted to the REE occurrences in the metamorphic hydrothermal systems of the Kuusamo Belt.

Supplementary Materials: The following are available online at <http://www.mdpi.com/2075-163X/8/8/356/s1>. Electron Probe Microanalysis; Table S1: Electron microprobe analyses (wt %) of ancyllite, monazite, bastnäsite, apatite allanite and xenotime from Sokli carbonatites, Table S2: Electron microprobe analyses (wt %) of ancyllite, bastnäsite, monazite and apatite from Korsnäs, Table S3: Electron microprobe analyses (wt %) of monazite, allanite, chevkinite, bastnäsite, synchysite and apatite from Kortejärvi and Laivajoki carbonatites, Table S4: Electron microprobe analyses (wt %) of fergusonite, allanite and columbite from Otanmäki, Table S5: Electron microprobe analyses (wt %) of REE minerals from Tana Belt, Table S6: Electron microprobe analyses (wt %) of REE, Y, Nb, U and Th-bearing minerals from Kuusamo Belt (Uuniniemi and Honkilehto), Table S7: Electron microprobe analyses (wt %) of REE-bearing minerals from Rapakivi granite, Table S8: Electron microprobe analyses (wt %) of monazite and thorite/huttonite from Kovala monazite bearing granite.

Author Contributions: T.A.-A. performed all analytical work and data processing, the authors (T.A.-A., F.M., and P.L.) discussed the results and wrote the article together, and S.L. conducted the field work, collected the samples analyzed, and studied jointly during the present project.

Funding: The APC was funded by the Geological Survey of Finland.

Acknowledgments: We are grateful to those who have provided help during the preparation of this paper, and particularly to Bo Johanson, Lassi Pakkanen and Sari Lukkari in the minerals laboratory of the Geological Survey of Finland (GTK) for help with electron microprobe and scanning electron microscope. Also we thanks Kirsti Keskisaari (GTK) for her assistance to preparation of maps. We thank two anonymous Minerals reviewers for their helpful comments which helped us improve this manuscript.

Conflicts of Interest: The authors declare no conflict of interest.

Appendix A

Analytical Methods

EPMA. Elemental maps and quantitative major and minor element analyses were made using a Cameca SX100 Electron Probe Micro Analyzer (EPMA) (GTK Electron optics and microanalysis Laboratory, Espoo, Finland) housed at the Geological Survey of Finland at Otaniemi, Espoo. X-ray maps of Y (TAP, $L\alpha$), Ce (LLIF, $L\alpha$), La (LLIF, $L\alpha$), U (PET, $M\alpha$) and Th (LPET, $M\alpha$) were made in stage scan mode using 20 kV accelerating voltage, 100 nA beam current and a dwell time of 100–200 ms. Quantitative analyses were performed on the same instrument. Operating conditions were: accelerating voltage = 20 kV, beam current = 6–60 nA and beam diameter = 1–10 μm . Lower beam currents and larger beam diameters were used for beam sensitive mineral phases. Elements were analyzed using following analyzing crystals: TAP for Si $K\alpha$, Si $K\beta$, Mg $K\alpha$, Al $K\alpha$, and Y $L\alpha$, LLIF for Fe $K\alpha$, Mn $K\alpha$, Ba $L\alpha$, Nd $L\beta$, Ce $L\alpha$, La $L\alpha$, Sm $L\beta$, Gd $L\beta$, Pr $L\beta$, Tb $L\beta$, Dy $L\beta$, Ho $L\beta$, Er $L\beta$, Yb $L\alpha$, and Lu $L\alpha$, Pc0 for Na $K\alpha$ and F $K\alpha$, LPET for Ca $K\alpha$, P $K\alpha$, Ti $K\alpha$, Cl $K\alpha$, U $M\beta$, Th $M\alpha$, Pb $M\beta$ and S $K\alpha$.

The standards were diopside (Astimex) for Si $K\alpha$, Si $K\beta$, Ca $K\alpha$ and Mg $K\alpha$, almandine garnet (Astimex) for Fe $K\alpha$ and Al $K\alpha$, tugtupite (Astimex) for Na $K\alpha$ and Cl $K\alpha$, fluorite (Astimex) for F $K\alpha$, rutile (Astimex) for Ti $K\alpha$, monazite (Astimex) for P $K\alpha$, Ce $L\alpha$, Nd $L\alpha$ and La $L\alpha$, Y-Al-garnet (Astimex) for Y $L\alpha$, rhodonite (Astimex) for Mn $K\alpha$, galena (Astimex) for Pb $M\beta$, Th (Astimex) and thorite (MAC) for Th $M\alpha$, U (Astimex) and U Ree glass (MAC) for U $M\beta$, barite (Astimex) for Ba $L\alpha$, Sm $L\beta$, Gd $L\beta$, Pr $L\beta$, Tb $L\beta$, Dy $L\beta$, Ho $L\beta$, Er $L\beta$, Yb $L\alpha$ and Lu $L\alpha$ were measured from a specific ReP5O14 set (ZSC).

Counting times at the peak position varied between 10 and 240 s depending on the analyzed mineral phase. Extra strontium caused by silica and extra phosphorus caused by calcium were corrected. The matrix correction method was Phi-Rho-Z. Accuracy of unknown analyses was checked routinely by analyzing our own Astimex- standards as unknowns.

References

1. Chakhmouradian, A.R.; Wall, F. Rare earth elements: Minerals, mines, magnets (and more). *Elements* **2012**, *8*, 333–340. [[CrossRef](#)]
2. Wall, F. Rare earth elements. In *Critical Metals Handbook*; Gunn, A.G., Ed.; John Wiley & Sons: Stanford, CA, USA, 2014; pp. 312–339.
3. Smith, M.P.; Henderson, P.; Campbell, L.S. Fractionation of the REE during hydrothermal processes: Constraints from the Bayan Obo Fe-REE-Nb deposit, Inner Mongolia, China. *Geochim. Cosmochim. Acta* **2000**, *64*, 3141–3160. [[CrossRef](#)]
4. Fan, H.R.; Yang, K.F.; Hu, F.F.; Liu, X.; Wang, K.Y. The giant Bayan Obo REE-Nb-Fe deposit, China: Controversy and ore genesis. *Geosci. Front.* **2016**, *7*, 335–344. [[CrossRef](#)]
5. Chakhmouradian, A.R.; Zaitsev, A.N. Rare earth mineralization in igneous rocks: Sources and processes. *Elements* **2012**, *8*, 347–353. [[CrossRef](#)]
6. Ling, M.X.; Liu, Y.L.; Williams, I.S.; Teng, F.Z.; Yang, X.Y.; Ding, X.; Wei, G.J.; Xie, L.H.; Deng, W.F.; Sun, W. Formation of the world's largest REE deposit through protracted fluxing of carbonatite by subduction-derived fluids. *Sci. Rep.* **2013**, *3*, 1776. [[CrossRef](#)]
7. Goodenough, K.M.; Schilling, J.; Jonsson, E.; Kalvige, P.; Charles, N.; Tuduri, J.; Deady, E.A.; Sadeghi, M.; Schiellerup, H.; Müller, A. Europe's rare earth element resource potential: An overview of REE metallogenetic provinces and their geodynamic setting. *Ore Geol. Rev.* **2016**, *72*, 838–856. [[CrossRef](#)]
8. Upton, B.G.J.; Emeleus, C.H.; Heaman, L.M.; Goodenough, K.M.; Finch, A.A. Magmatism of the mid-Proterozoic Gardar Province, South Greenland: Chronology, petrogenesis and geological setting. *Lithos* **2003**, *68*, 43–65. [[CrossRef](#)]
9. Andreasson, P.G.; Rodhe, A. Geology of the Protogine Zone south of Lake Vättern, southern Sweden: A re-interpretation. *Fören. Stockholm Förh* **1990**, *111*, 107–125. [[CrossRef](#)]
10. Wall, F.; Zaitsev, A.N. *Phoscorites Carbonatites from Mantle to Mine: The Key Example of the Kola Alkaline Province*; Mineralogical Society of Series; Mineralogical Society: London, UK, 2004; Volume 10, p. 498.
11. Zaitsev, A.N.; Williams, C.T.; Jeffries, T.E.; Strekopytov, S.; Moutte, J.; Ivashchenkova, O.V.; Spratt, J.; Petrov, S.V.; Wall, F.; Seltmann, R. Reprint of rare earth elements in phoscorites and carbonatites of the Devonian Kola Alkaline Province, Russia: Examples from Kovdor, Khibina, Vuoriyarvi and Turiy Mys complexes. *Ore Geol. Rev.* **2015**, *64*, 477–498. [[CrossRef](#)]
12. Sarapää, O.; Al Ani, T.; Lahti, S.I.; Sarala, P.; Torppa, A.; Kontinen, A. Rare earth exploration potential in Finland. *J. Geochem. Explor.* **2013**, *133*, 25–41. [[CrossRef](#)]
13. Sarapää, O.; Lauri, L.S.; Ahtola, T.; Al Ani, T.; Grönholm, S.; Kärkkäinen, N.; Lintinen, P.; Torppa, A.; Turunen, P. *Discovery Potential of Hi-Tech Metals and Critical Minerals in Finland*; Report of Investigation; Geological Survey of Finland: Espoo, Finland, 2015; Volume 219, pp. 1–54.
14. Tichomirowa, M.; Grosche, G.; Gotze, J.; Belyatsky, B.V.; Savva, E.V.; Keller, J.; Todt, W. The mineral isotope composition of two Precambrian carbonatite complexes from the Kola alkaline province—Alteration versus primary magmatic signatures. *Lithos* **2006**, *91*, 229–249. [[CrossRef](#)]
15. Rukhlov, A.S.; Bell, K. Geochronology of carbonatites from the Canadian and Baltic shields, and the Canadian cordillera: Clues to mantle evolution. *Miner. Petrol.* **2010**, *98*, 11–54. [[CrossRef](#)]
16. Eilu, P. *Mineral Deposits and Metallogeny of Fennoscandia*; Special Paper; Geological Survey of Finland: Espoo, Finland, 2012; Volume 53, p. 401.
17. Al-Ani, T. *Mineralogy and Petrography of Siilinjärvi Carbonatite and Glimmerite Rocks, Eastern Finland*; Report of Investigation, 164/2013; Geological Survey of Finland: Espoo, Finland, 2013; 15p. Available online: http://tupa.gtk.fi/raportti/arkisto/164_2013.pdf (accessed on 6 August 2018).
18. Korsman, K.; Koistinen, T.; Kohonen, J.; Wennerström, M.; Ekdahl, E.; Honkamo, M.; Idman, H.; Pekkala, Y. *Bedrock Map of Finland 1:1,000,000*; Report of Investigation; Geological Survey of Finland: Espoo, Finland, 1997.
19. Nironen, M.; Kousa, J.; Luukas, J.; Lahtinen, R. *Geological Map of Finland—Bedrock. 1:1,000,000*; Report of Investigation; Geological Survey of Finland: Espoo, Finland, 2016.
20. Vartiainen, H.; Paarma, H. Geological characteristics of the Sokli carbonatite complex, Finland. *Econ. Geol.* **1979**, *74*, 1296–1306. [[CrossRef](#)]

21. Kramm, U.; Kogarko, L.N.; Kononova, V.A.; Vartiainen, H. The Kola alkaline province of the CIS and Finland: Precise Rb–Sr ages define 380–360 Ma age range for all magmatism. *Lithos* **1993**, *30*, 33–44. [[CrossRef](#)]
22. Korsakova, M.; Krasotkin, S.; Stromov, V.; Iljina, M.; Lauri, L.; Nilsson, P. Metallogenic areas in Russian part of the Fennoscandian shield. In *Mineral Deposits and Metallogeny of Fennoscandia: Geological Survey of Finland; Special Paper*; Eilu, P., Ed.; Geological Survey of Finland: Espoo, Finland, 2012; Volume 53, pp. 343–395.
23. Vartiainen, H. The petrography, mineralogy and petrochemistry of the Sokli carbonatite massif northern Finland. *Bull. Geol. Surv. Finl.* **1980**, *313*, 126.
24. Vartiainen, H.; Vitikka, A. The late stage dikes of the Sokli massif and their tectonic control. *Geochem. Int.* **1994**, *31*, 103–106.
25. Al-Ani, T.; Sarapää, O. Geochemistry and mineral phases of REE in Jammi carbonatite veins and fenites, southern end of the Sokli complex, NE Finland. *Geochem. Explor. Environ. Anal.* **2013**, *13*, 217–224. [[CrossRef](#)]
26. Elliott, H.A.L.; Walla, F.; Chakhmouradian, A.R.; Siegfried, P.R.; Dahlgren, S.; Weatherley, S.; Finch, A.A.; Marksg, M.A.W.; Dowman, E.; Deady, E. Fenites associated with carbonatite complexes: A review. *Ore Geol. Rev.* **2018**, *93*, 38–59. [[CrossRef](#)]
27. Lehtonen, M.I.; Kujala, H.; Kärkkäinen, N.; Lehtonen, A.; Mäkitie, H.; Mänttari, I.; Virransalo, P.; Vuokko, J. *The Bedrocks of Southern Ostrobothnian Schist Belt*; Report of Investigation; Geological Survey of Finland: Espoo, Finland, 2005; p. 158.
28. Al-Ani, T.; Konnunaho, K.; Sarapää, O. *Microprobe Analysis on REE-Minerals of Enontekiö (Palkiskuru and Palovaara) and Kuusamo (Honkilehto) Hydrothermal Mineralization and Kortejärvi-Laijavajoki Carbonatites, Northern Finland*; Report M42/2010/66; Geological Survey of Finland: Espoo, Finland, 2010; p. 20.
29. Papunen, H.; Gorbunov, G. *Nickel Copper Deposits of the Baltic Shield and Scandinavian Caledonides*; Geological Survey of Finland: Espoo, Finland, 1985; Volume 333, p. 394.
30. Huhma, H.; Eero Hanski, E.; Vuollo, J. Sm–Nd isotopes in Paleoproterozoic mafic rocks in Finland—Range of ages, mantle sources and crust–mantle interaction. *Bull. Geol. Surv. Finl.* **2006**, *1*, 54.
31. Nykänen, J.; Laajoki, K.; Karhu, J. Geology and geochemistry of the early Proterozoic Kortejärvi and Laijavajoki carbonatites, central Fennoscandian Shield, Finland. *Bull. Geol. Soc. Finl.* **1997**, *69*, 5–30. [[CrossRef](#)]
32. Huhma, H.; Eero Hanski, A.; Vuollo, J.; Mänttari, I.; Lahaye, Y. *Sm–Nd and U–Pb Isotope Geochemistry of the Palaeoproterozoic Mafic Magmatism in Eastern and Northern Finland*; Geological Survey of Finland: Espoo, Finland, 2018; Volume 405, 150p.
33. Lindholm, O.; Anttonen, R. Geology of the Otanmäki mine. In *Precambrian Ores of Finland, 26th International Geological Congress, Guide to Excursions 078A+C, Part 2 (Finland)*; Häkli, T.A., Ed.; Geological Survey of Finland: Espoo, Finland, 1980; pp. 25–33.
34. Talvitie, J.; Paarma, H. Precambrian basic magmatism and the Ti–Fe ore formation in central and northern Finland. *Bull. Geol. Surv. Finl.* **1980**, *307*, 98–107.
35. Puustinen, K. *The Finnish Mining Industry and Production of Mineral Raw Materials in the Period 1530–2001, A Historical Overview of Production*; Archive Report; Geological Survey of Finland: Espoo, Finland, 2003; p. 578.
36. Lahtinen, R. *Main Geological Features of Fennoscandia*; Special Paper; Geological Survey of Finland: Espoo, Finland, 2012; Volume 53, pp. 13–18.
37. Hugg, R.; Heiskanen, V. *Exploration of Nb–La Deposits in Otanmäki Area*; Report OU 28/85; Rautaruukki CO. Ore Exploration: Oulu, Finland, 1986; p. 14.
38. Salminen, R.; Tarvainen, T. Geochemical mapping and databases in Finland. In *Geochemical exploration 1993*. *J. Geochem. Explor.* **1995**, *55*, 321–327. [[CrossRef](#)]
39. Rasilainen, K.; Lahtinen, R.; Bornhorst, T.J. *Chemical Characteristics of Finnish Bedrock—1:1,000,000 Scale Bedrock Map Units*; Report of Investigation; Geological Survey of Finland: Espoo, Finland, 2008; Volume 171, p. 94.
40. Sarapää, O.; Sarala, P. Rare earth element and gold exploration in glaciated terrain: Example from the Mäkärä area, Northern Finland. *Geochem. Explor. Environ. Anal.* **2013**, *13*, 131–143. [[CrossRef](#)]
41. Salmirinne, H.; Turunen, P.; Sarapää, O. *On Prospecting for REE in the Tana Belt, Northern Finland*; Report of Investigation; Geological Survey of Finland: Espoo, Finland, 2013; Volume 198, pp. 152–155.
42. Tuisku, P.; Huhma, H. Evolution of migmatitic granulite complexes: Implications from Lapland Granulite Belt, part II: Isotopic dating. *Bull. Geol. Soc. Finl.* **2006**, *78*, 143–175. [[CrossRef](#)]
43. Cagnard, F.; Barbey, P.; Garpais, D. Transition between “Archaean-type” and “modern-type” tectonics: Insights from the Finnish Lapland Granulite Belt. *Precambrian Res.* **2011**, *187*, 127–142. [[CrossRef](#)]

44. Al-Ani, T.; Sarapää, O. *REE-Mineralogy of Arkosic Gneisses from Mäkärä-Vaulo Area, Tana Belt, Northern Finland*; Investigation Report 74/2012; Geological Survey of Finland: Espoo, Finland, 2012; p. 36.
45. Heilimo, E.; Halla, J.; Lauri, L.S.; Rämö, O.T.; Huhma, H.; Kurhila, M.I.; Front, K. The Paleoproterozoic Nattanen-type granites in northern Finland and vicinity—A post collisional oxidized A-type suite. *Bull. Geol. Soc. Finl.* **2009**, *81*, 7–38. [[CrossRef](#)]
46. Berger, A.; Gnos, E.; Janots, E.; Fernandez, A.; Giese, J. Formation and composition of rhabdophane, bastnäsite and hydrated thorium minerals during alteration: Implications for geochronology and low-temperature processes. *Chem. Geol.* **2008**, *254*, 238–248. [[CrossRef](#)]
47. Buda, G.; Nagy, G.; Pál-Molnár, E. Allanite and monazite occurrences in Variscan granitoids of Tisza Mega-Unit (South Hungary). *Carpathian J. Earth Environ. Sci.* **2014**, *9*, 57–68.
48. Budzyń, B.; Hetherington, C.J.; Williams, M.L.; Jercinovic, M.J.; Michalik, M. Fluid mineral interactions and constraints on monazite alteration during metamorphism. *Miner. Mag.* **2010**, *74*, 659–681. [[CrossRef](#)]
49. Förster, H.J. Cerite-(Ce) and thorian synchysite-(Ce) from the Niederbobritzsch granite, Erzgebirge, Germany: Implications for the differential mobility of the LREE and Th during alteration. *Can. Miner.* **2000**, *38*, 67–79. [[CrossRef](#)]
50. Hirtopanu, P.; Andersen, J.C.; Fairhurst, R.J.; Jakab, G. Allanite-(Ce) and its associations, from the Ditrau alkaline intrusive massif, East Carpathians, Romania. *Proc. Romanian Acad. Ser.* **2013**, *15*, 59–74.
51. Buda, G.; Nagy, G. Some REE-bearing accessory minerals in two types of Variscan granitoids, Hungary. *Geol. Carpathica* **1995**, *46*, 67–78.
52. Meintzer, R.E.; Mitchell, R.S. The epigene alteration of allanite. *Can. Miner.* **1988**, *26*, 945–955.
53. Wing, B.A.; Ferry, J.M.; Harrison, T.M. Prograde destruction and formation of monazite and allanite during contact and regional metamorphism of pelites: Petrology and geochronology. *Contrib. Miner. Pet.* **2003**, *145*, 228–250. [[CrossRef](#)]
54. Hanson, S.L.; Falster, A.U.; Simmons, W.B.; Brown, T.J.A. Allanite-(Nd) from the Kingman feldspar mine, Mojave pegmatite district, Northwester Arizona, USA. *Can. Miner.* **2012**, *50*, 815–824. [[CrossRef](#)]
55. Pankka, H.S.; Vanhanen, E.J. Early Proterozoic Au-Co-U mineralization in the Kuusamo district, Northeastern Finland. *Precambrian Res.* **1992**, *58*, 387–400. [[CrossRef](#)]
56. Frietsch, R.; Tuisku, P.; Martinsson, O.; Perdahl, J.-A. Early Proterozoic Cu-(Au) and Fe ore deposits associated with regional Na-Cl metasomatism in northern Fennoscandia. *Ore Geol. Rev.* **1997**, *12*, 1–34. [[CrossRef](#)]
57. Vanhanen, E. Geology, mineralogy and geochemistry of the Fe-Co-Au-(U) deposits in the Paleoproterozoic Kuusamo Schist Belt, Northeastern Finland. *Bull. Geol. Surv. Finl.* **2001**, *399*, 229.
58. Mutanen, T. *Alkaline and Appinitic Rocks. Report on the Project Magmatism and Ore formation 2002–2005*; Report 9/2011, (Finnish with English abstract); Geological Survey of Finland: Espoo, Finland, 2011; p. 627.
59. Pankka, H. Geology and Mineralogy of Au-Co-U Deposits in the Proterozoic Kuusamo. Volcano Sedimentary Belt, Northeastern Finland. Ph.D. Thesis, Michigan Technological University, Houghton, MI, USA, 1992; p. 233.
60. Rämö, O.T.; Haapala, I. Rapakivi granites. *Precambrian Geology of Finland, Key to the Evolution of the Fennoscandian Shield. Dev. Precambrian Geol.* **2005**, *14*, 533–562. [[CrossRef](#)]
61. Haapala, I. Petrography and geochemistry of the Eurajoki stock, a rapakivi-granite complex with greisen-type mineralization in Southwestern Finland. *Bull. Geol. Surv. Finl.* **1977**, *286*, 128.
62. Al-Ani, T.; Ahtola, T.; Kuusela, J. *Critical Metals Mineralization in the Late-Stage Intrusions of Vyborg Batholith, Southern Finland*; Report of Investigation 21/2017; Geological Survey of Finland: Espoo, Finland, 2017; p. 39.
63. Al-Ani, T.; Ahtola, T.; Kuusela, J.; Al-Ansari, N. Mineralogical and petrographic characteristics of indium and REE-bearing accessory phases in the Kymi Granite Stock, Southern Finland. *Nat. Resour.* **2018**, *9*, 23–41. [[CrossRef](#)]
64. Lukkari, S.; Thomas, R.; Haapala, I. Crystallization of the Kymi topaz granite stock within the Vyborg rapakivi granite batholith, Finland: Evidence from melt inclusions. *Can. Miner.* **2009**, *47*, 1359–1374. [[CrossRef](#)]
65. Al-Ani, T. REE-bearing minerals in the Rapakivi Granite, Southern Finland. *Open Geosci.* **2015**, *7*, 646–662. [[CrossRef](#)]
66. Hölttä, P.; Huhma, H.; Mänttari, I.; Paavola, J. P-T-t development of Archaean granulites in Varpaisjärvi, central Finland. II. Dating of high-grade metamorphism with the U-Pb and Sm-Nd methods. *Lithos* **2000**, *50*, 121–136. [[CrossRef](#)]

67. Pabst, A.; Hutton, C.O. Huttonite, a new monoclinic thorium silicate, with an account on its occurrence, analysis, and properties. *Am. Miner.* **1951**, *36*, 60–65.
68. Linthout, K. Tripartite division of the system $2\text{REEPO}_4\text{-CaTh}(\text{PO}_4)_2\text{-2ThSiO}_4$, discreditation of brabantite, and recognition of cheralite as the name for members dominated by $\text{CaTh}(\text{PO}_4)_2$. *Can. Miner.* **2007**, *45*, 503–508. [[CrossRef](#)]
69. Förster, H.J.; Harlov, D.E. Monazite-(Ce) huttonite solid solutions in granulite-facies metabasites from the Ivrea-Verbano Zone, Italy. *Miner. Mag.* **1999**, *63*, 587–594. [[CrossRef](#)]
70. Overstreet, W.C. The geological occurrence of monazite. *Geol. Surv. Prog. Pap.* **1967**, *530*, 327.
71. Mohr, D.W. Zoned porphyroblasts of metamorphic monazite in the Anakeesta Formation, Great Smoky Mountains, North Carolina. *Am. Miner.* **1984**, *69*, 98–103.
72. Kelly, N.M.; Harley, S.L.; Möller, A. Complexity in the behaviour and recrystallization of monazite during high-T metamorphism and fluid infiltration. *Chem. Geol.* **2012**, *322–323*, 192–208. [[CrossRef](#)]
73. McDonough, W.F.; Sun, S.S. Composition of the Earth. *Chem. Geol.* **1995**, *120*, 223–253. [[CrossRef](#)]
74. Hughes, J.M.; Mariano, A.N. The crystal chemistry of monazite and xenotime. *Am. Miner.* **1995**, *80*, 21–26.
75. Haas, J.R.; Shock, E.L.; Sassani, D.C. Rare earth elements in hydrothermal systems: Estimates of standard partial modal thermodynamic properties of aqueous complexes of the rare earth elements at high pressures and temperatures. *Geochim. Cosmochim. Acta* **1995**, *59*, 4329–4350. [[CrossRef](#)]
76. Bagiński, B.; Macdonald, R.; Dzierżanowski, P.; Zozulya, D.; Kartashov, P.M. Hydrothermal alteration of chevkinite-group minerals: Products and mechanisms. Part 1. Hydration of chevkinite-(Ce). *Miner. Mag.* **2015**, *79*, 1039–1059. [[CrossRef](#)]
77. Macdonald, R.; Bagiński, B.; Kartashov, P.M.; Zozulya, D.; Dzierżanowski, P. Hydrothermal alteration of chevkinite-group minerals. Part 2. Metasomatite from the Keivy massif, Kola Peninsula, Russia. *Miner. Mag.* **2015**, *79*, 1019–1037. [[CrossRef](#)]
78. Grammatikopoulos, T.; Mercer, W.; Gunning, C.; Prout, S. Quantitative characterization of the REE minerals by QEMSCAN from the Nechalacho Heavy Rare Earth Deposit, Thor Lake Project, NWT, Canada. *SGS Miner. Serv. Tech. Pap.* **2011**, *7*, 1–11.
79. Andersson, S.S.; Wagner, T.; Jonsson, E.; Michallik, R.M. Mineralogy, paragenesis and mineral chemistry of REEs in the Olserum-Djupedal REE-phosphate mineralization, SE Sweden. *Am. Miner.* **2018**, *103*, 125–142. [[CrossRef](#)]
80. Hanson, S.L.; Simmons, W.B.; Webber, K.L.; Falster, A.U. Rare-earth-element mineralogy of granitic pegmatites in the Trout Creek Pass District, Chaffee County, Colorado. *Can. Miner.* **1992**, *30*, 673–686.
81. Papoutsas, A.; Pe-Piper, G. The relationship between REE-Y-Nb-Th minerals and the evolution of an A-type granite, Wentworth Pluton, Nova Scotia. *Am. Miner.* **2013**, *98*, 444–462. [[CrossRef](#)]
82. Holtstam, D.; Andersson, U.B. The REE minerals of the Bastnäs-type deposits, South-Central Sweden. *Can. Miner.* **2007**, *45*, 1073–1114. [[CrossRef](#)]

